Int. J. Mol. Sci. **2012**, *13*, 15420-15446; doi:10.3390/ijms131115420

OPEN ACCESS
International Journal of
Molecular Sciences
ISSN 1422-0067
www.mdpi.com/journal/ijms

Article

Errors in the Calculation of ^{27}Al Nuclear Magnetic Resonance Chemical Shifts

Xianlong Wang [1,2,*], Chengfei Wang [1] and Hui Zhao [1]

[1] Center of Bioinformatics, University of Electronic Science and Technology of China, No. 4, 2nd Section, Jianshe Road, Chengdu 610054, China;
E-Mails: chengfeiwang.aka.chance@gmail.com (C.W.); kathy517413@sohu.com (H.Z.)

[2] Department of Chemistry, Bryn Mawr College, 101 North Merion Avenue, Bryn Mawr, PA 19010, USA

* Author to whom correspondence should be addressed; E-Mail: WangXianlong@uestc.edu.cn; Tel.: +86-28-8320-8232; Fax: +86-28-8320-8238.

Received: 10 October 2012; in revised form: 2 November 2012 / Accepted: 6 November 2012 / Published: 21 November 2012

Abstract: Computational chemistry is an important tool for signal assignment of ^{27}Al nuclear magnetic resonance spectra in order to elucidate the species of aluminum(III) in aqueous solutions. The accuracy of the popular theoretical models for computing the ^{27}Al chemical shifts was evaluated by comparing the calculated and experimental chemical shifts in more than one hundred aluminum(III) complexes. In order to differentiate the error due to the chemical shielding tensor calculation from that due to the inadequacy of the molecular geometry prediction, single-crystal X-ray diffraction determined structures were used to build the isolated molecule models for calculating the chemical shifts. The results were compared with those obtained using the calculated geometries at the B3LYP/6-31G(d) level. The isotropic chemical shielding constants computed at different levels have strong linear correlations even though the absolute values differ in tens of ppm. The root-mean-square difference between the experimental chemical shifts and the calculated values is approximately 5 ppm for the calculations based on the X-ray structures, but more than 10 ppm for the calculations based on the computed geometries. The result indicates that the popular theoretical models are adequate in calculating the chemical shifts while an accurate molecular geometry is more critical.

Keywords: aluminum-27 NMR; aluminum(III) complexes; computational chemistry; density functional theory

1. Introduction

Studies with aluminum(III) (Al(III)) complexes are important in bioinorganic chemistry, geochemistry, environmental science, and material science due to the toxic effects of many aluminum compounds and their industrial usage as catalysts and coagulation agents. Because various kinds of species of Al(III) might differ significantly in their toxic effects, speciation of aqueous Al(III) complexes is of great value to study their biological and environmental roles [1,2]. Nuclear magnetic resonance spectroscopy (NMR) has been routinely used in studying the coordination chemistry and speciation of Al(III) in aqueous solutions due to its noninvasive character [3].

^{1}H, ^{13}C, ^{17}O and ^{27}Al are commonly used nuclei for observing NMR spectra of Al(III) complexes. Among them, ^{27}Al possesses advantages over the others, including 100% abundance, high signal sensitivity, a wide range of chemical shifts, and sensitivity to coordination environment. For example, the ^{27}Al chemical shift (δ_{Al}) of the tetrahedral $[Al(OH)_4]^-$ species is 80 ppm relative to the octahedral $[Al(OH_2)_6]^{3+}$ species. Therefore, solution-state ^{27}Al NMR spectroscopy has been a very powerful tool to characterize the structures of Al(III) complexes, to monitor the hydrolysis of Al(III), to identify Al(III) species in biological and environmental samples, and to quantify the concentrations of Al(III) species [3]. It is particularly useful for the characterization of those species which are difficult to isolate and/or to crystallize or inert for other spectroscopic methods.

^{27}Al nucleus has a spin of 5/2 and with a moderately large electric quadrupole moment. Both the chemical shift and line width of ^{27}Al signals are sensitive to aluminum coordination geometry. For a highly asymmetric coordination geometry, the resonance peaks of ^{27}Al may be too broad to observe. In aqueous solutions, the coordination number of Al^{3+} monomers fluctuates between 4 and 6. Many aqueous Al(III) complexes are octahedral-coordinated and some may be distorted. As a result, δ_{Al} of these complexes are not far away from 0 ppm relative to the aqueous $[Al(OH_2)_6]^{3+}$ species and the chemical shift spectra peaks are not sharp. Furthermore, due to the tendency of Al(III) to hydroxylize, to oligomerize and to form mixed complexes, the solutions are often a complicated system with many coexisting species. Often, many ^{27}Al chemical shift signals are crowded together in the vicinity of 0 ppm. Although tentative structural information can be made by comparing the spectroscopic features of the unknown species with model complexes, it is usually difficult to make unique assignments. Therefore, computational modeling, along other experimental methods, is often used to complement ^{27}Al NMR experiments.

With the rapid development of computational chemistry, its application has become almost ubiquitous in all branches of chemistry. In the study of Al(III) complexes, computational methods have been used to predict NMR spectra. For example, Tossell [4] calculated the chemical shieldings of ^{27}Al, along with other nuclei, by applying the gauge-including atomic orbital (GIAO) method [5,6] with the Hartree-Fock (HF) theory and to elucidate the species formed during the hydrolysis and the oligomerization process of Al(III) in aqueous solution. Amini *et al.* [7,8] applied the HF theory and

density functional theory (DFT) to calculate the solid-state ^{27}Al NMR spectra of aluminum acetylacetonate and other similar complexes for the clarification of the crystal structure of the compounds. Mirzaei *et al.* [9,10] used DFT calculations to calculate ^{27}Al and ^{31}P chemical shieldings in the investigation of aluminum phosphide and nitride nanotubes. The gauge including projected augmented wave (GIPAW) method [11] developed by Mauri and Pickard in 2001 [12] which enabled the calculation of all-electron NMR parameters in solids was also used to predict the solid-state ^{27}Al NMR spectra [13,14].

Although the calculations of chemical shieldings have played an important role in the determination of structures, there have been a limited number of systematic studies concerned with the accuracy of computational models that predict the chemical shifts of ^{27}Al. Mulder *et al.* [15] reviewed several theoretical methods for the calculation of NMR chemical shifts and they evaluated the applications of these methods in protein structure determination. Jensen [16] evaluated the basis set convergence problem in calculating NMR shielding constants calculated by two DFT methods and proposed to use pcS-*n* basis sets for calculating shielding constants. In 1999, Kubicki *et al.* [17] performed a thorough computational study on Al(III) hydrolysis products and Al(III)-carboxylate complexes to determine how accurately the ^{27}Al chemical shifts can be calculated using *ab initio* methods. The study was based on the self-consistent isodensity polarized continuum model (SCIPCM) of the aqueous species using HF and second-order Møller-Plesset perturbation (MP2) theories. By comparing the calculated chemical shifts with the experimental values, they suggested that the ^{27}Al NMR spectra should be reinterpreted in some previous publications. Ten years later, Bi *et al.* [18] assessed the accuracy of ^{27}Al chemical shift calculations that used 29 DFT functionals, HF and MP2 models. They concluded that of all the models, the HF and MP2 models gave the most accurate results. Their conclusion was made on the basis of the calculations of only a few Al(III) hydrolysis products. It remains unanswered if the conclusion holds for more general Al(III) complexes.

Previous studies found that the error involved in the *ab initio* calculation of ^{27}Al chemical shifts is typically approximately 10 ppm and for some DFT models it could be as large as 30 ppm [18]. Errors of such magnitude pose serious limitations for the application in assigning experimental spectra, since the ^{27}Al chemical shifts of many octahedral-coordinated complexes are typically distributed in the small range from −10 to 30 ppm. To distinguish between the small differences found in similar complexation species, a computational method must be able to reproduce the chemical shifts with an error within a few ppm and at least be able to put the resonance peaks in the correct order.

There are two major parts to the errors in calculated ^{27}Al chemical shifts: the error in the prediction of the geometry and the error in the chemical shielding determination. Previous studies presenting the calculations of ^{27}Al chemical shifts did not differentiate between these two kinds of errors. There have been many publications concerning the accuracy of *ab initio* models including those that use DFT in predicting complex geometries [19]. The purpose of this work is to evaluate the performance of several commonly used theoretical models, including HF, MP2 and DFT, in predicting the chemical shifts of Al(III) complexes. Our approach is to use the X-ray crystallographic structures to calculate the chemical shifts and then to compare them with the experimentally measured values. It has been well established that X-ray diffraction structures represent well the molecular geometries in solutions except for the rotation-flexible functional groups.

2. Results and Discussion

More than 200 single-crystal X-ray diffraction determined geometries [20–145] of 114 Al(III) complex species were obtained from the Cambridge Crystal Database. (There is more than one crystal structure available for some complexes.) In most species, Al(III) is found in an octahedral-coordination environment binding with six ligands or functional groups. Some Al(III) are found in tetrahedral coordination environments and a limited number of species are in penta-coordination environments. Usually Al(III) binds with ligands via O atoms. Al–N ranks second in the binding modes. A few species of Al(III) coordinated with fluorides and phosphates were also examined. This covers most coordination forms commonly encountered in the study of solution aluminum chemistry. Other coordination forms, such as planar tri-coordination and complexation with other ligands, e.g., H and Cl, were not studied in this work.

Figure 1. Correlation between the calculated isotropic ^{27}Al chemical shielding constants using the X-ray crystallographic geometries at the B3LYP/6-31G(d) (black squares) and the HF/6-311+G(d,p) (red circles) levels *versus* those obtained at the B3LYP/6-311+G(d,p) level. The black dashed line and the red dashed line are the best-fit linear regression of the two data sets, respectively, and the best-fit equations are given in Equations 1 and 2. The solid black line is the ideal diagonal line ($y = x$).

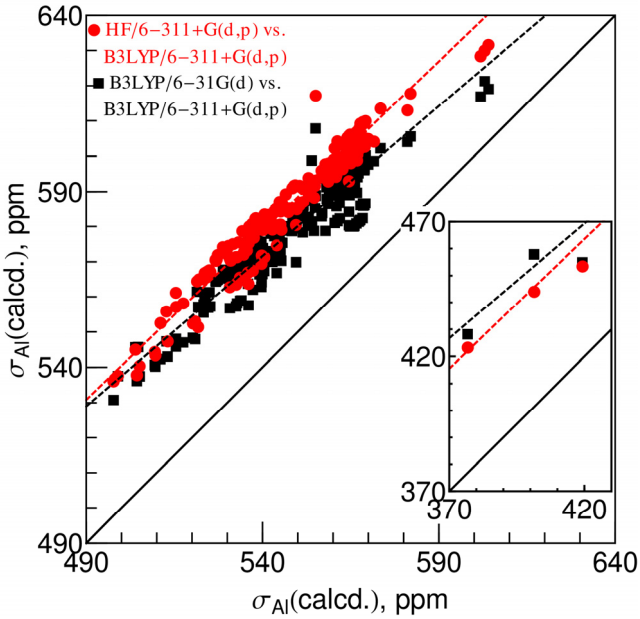

$$\sigma_{Al}\text{ (GIAO-B3LYP/6-31G(d))} = 114.1 + 0.85\ \sigma_{Al}\text{ (GIAO-B3LYP/6-311+G(d,p))},\ R^2 = 0.95 \quad (1)$$

$$\sigma_{Al}\text{ (GIAO-HF/6-311+G(d,p))} = 59.4 + 0.96\ \sigma_{Al}\text{ (GIAO-B3LYP/6-311+G(d,p))},\ R^2 = 0.98 \quad (2)$$

2.1. Chemical Shielding Constants

The chemical shielding tensors of each structure were calculated with the GIAO formalism [5,6] at the following four popular model levels, B3LYP/6-31G(d), HF/6-31G(d), B3LYP/6-311+G(d,p) and HF/6-311+G(d,p). In addition, MP2/6-311+G(d,p) was also applied to species of $[Al(OH_2)_6]^{3+}$, $[AlF_6]^{3-}$ and $[AlF_5(OH_2)]^{2-}$.

Figure 1 shows how the calculated isotropic shielding constants at different levels are correlated. The *x*-axis represents the values calculated at the B3LYP/6-311+G(d,p) level. On the *y*-axis direction, the shielding constants obtained at the B3LYP/6-31G(d), and HF/6-311+G(d,p) levels are represented as black squares and red circles, respectively. There is a strong linear correlation in a wide range from 350 to 600 ppm for both data sets, though the chemical shieldings calculated at different levels of theory could differ as large as 60 ppm. In general, the hybrid B3LYP functional gives consistently smaller shielding constants than the HF theory and so does the larger basis set (6-311+G(d,p)) than the smaller (6-31G(d)) basis set.

Comparing the two differently sized basis sets, 6-31G(d) *versus* 6-311+G(d,p), both using the B3LYP model, the coefficient of determination (R^2) of the linear regression is 0.95. The best-fit straight line is Equation 1 (black dashed line in Figure 1). The majority of the absolute fitting residuals (74%) are less than 5 ppm. There is one outlier point with a fitting residual of 24 ppm, while all the rest are less than 13 ppm. The outlier point is an Al-phosphate species. The exact reason for the outlier is unclear.

The shielding constants obtained at the HF/6-311+G(d,p) level are slightly higher than those at the B3LYP/6-31G(d) level. They also have strong linear correlations with the values obtained at the B3LYP/6-311+G(d,p) level (R^2 = 0.98). The best-fit straight line is Equation 2 (red dashed line in Figure 1). Most of the absolute fitting residuals (85%) are less than 5 ppm, while the rest are within 11 ppm except the Al-phosphate species which has a large residual of 24 ppm. For the calculations using the 6-31G(d) basis set, the correlation between the B3LYP and HF models is also strongly linear (R^2 = 0.99). Most of the fitting residuals are also within 5 ppm.

A more comprehensive study including the calculations with Dunning's correlation consistent basis sets [146,147], aug-cc-pV*X*Z (*X* = D, T and Q), was carried out for a limit number of complexes. The calculated shielding constants were shown in Figure 2. It is clear that the values did not converge well even at the aug-cc-pVTZ or aug-cc-pVQZ level for many geometries. However, the shielding constants calculated with different basis sets are highly correlated, which is consistent with the above observation. Jensen [16] proposed to use pcS-*n* basis sets with DFT methods to obtain the converged shielding constants. Here, we showed that even though there are large errors involved in the absolute shielding constants calculated with the commonly used basis sets, such as 6-31G(d) and 6-311+G(d,p), the errors are not random and a linear relationship exists between the values obtained with these small size basis sets and basis set limits. Therefore, these basis sets are still valuable in predicting ^{27}Al chemical shifts.

The MP2 model has been considered a more accurate model in electronic structure calculations. We also calculated the chemical shielding constants using this model with the 6-311+G(d,p) basis set. Because the large memory cost required and CPU time needed for the model, the calculations were done only for three species, $[Al(OH_2)_6]^{3+}$, $[AlF_6]^{3-}$ and $[AlF_5(OH_2)]^{2-}$. The calculated chemical shielding constants are also strongly correlated with the values obtained at the B3LYP/6-311+G(d,p) level, R^2 = 0.97. The slope of the best-fit equation is 0.98. The calculations indicate a trend, but more than three data sets (species) will have to be investigated before more firm quantitative relationships can be established.

Figure 2. Calculated ^{27}Al shielding constants using the GIAO method with the B3LYP functional with different basis sets in optimized geometries of $[Al(OH_2)_6]^{3+}$ (**A**), $[Al(OH)_4]^-$ (**B**) and other complexes (**C**). The basis sets were labeled on the graphs. In Panels **A** and **B**, there are three data points for each basis set which represent the values calculated in vacuum, in the PCM environment of water and methanol. Twelve geometries in **A** were obtained at the B3LYP/aug-cc-pVQZ, B3LYP/aug-cc-pVTZ, B3LYP/aug-cc-pVDZ and B3LYP/6-311++G(d,p) levels in vacuum, in the PCM environment of methanol and water, and the data sets are colored in black, red, blue, green, cyan, magenta, yellow, brown, orange, pink, purple and gray, respectively. The last geometry in **A**, which is in light orange color, was obtained at the B3LYP/6-31G(d) level in the PCM environment of water. Ten geometries in **B** were obtained at the B3LYP/aug-cc-pVQZ, B3LYP/aug-cc-pVTZ, B3LYP/aug-cc-pVDZ and B3LYP/6-311++G(d,p) levels in vacuum, at the B3LYP/aug-cc-pVQZ and B3LYP/aug-cc-pVTZ levels in the PCM environment of methanol, and at the B3LYP/aug-cc-pVQZ, B3LYP/aug-cc-pVTZ, B3LYP/aug-cc-pVDZ and B3LYP/6-31G(d) levels in the PCM environment of water, and the data sets are colored in black, red, blue, green, cyan, magenta, yellow, brown, orange and pink, respectively. Six complexes in **C** are $[Al(oxalate)_3]^{3-}$, $[AlF_6]^{3-}$, $[Al(EDTA)]^-$, $Al(lactate)_3$, $[Al(malonate)_2(OH_2)_2]^-$ and $[Al(N{\equiv}CCH_3)_6]^{3+}$, respectively. All the values obtained with a same geometry are connected with straight lines.

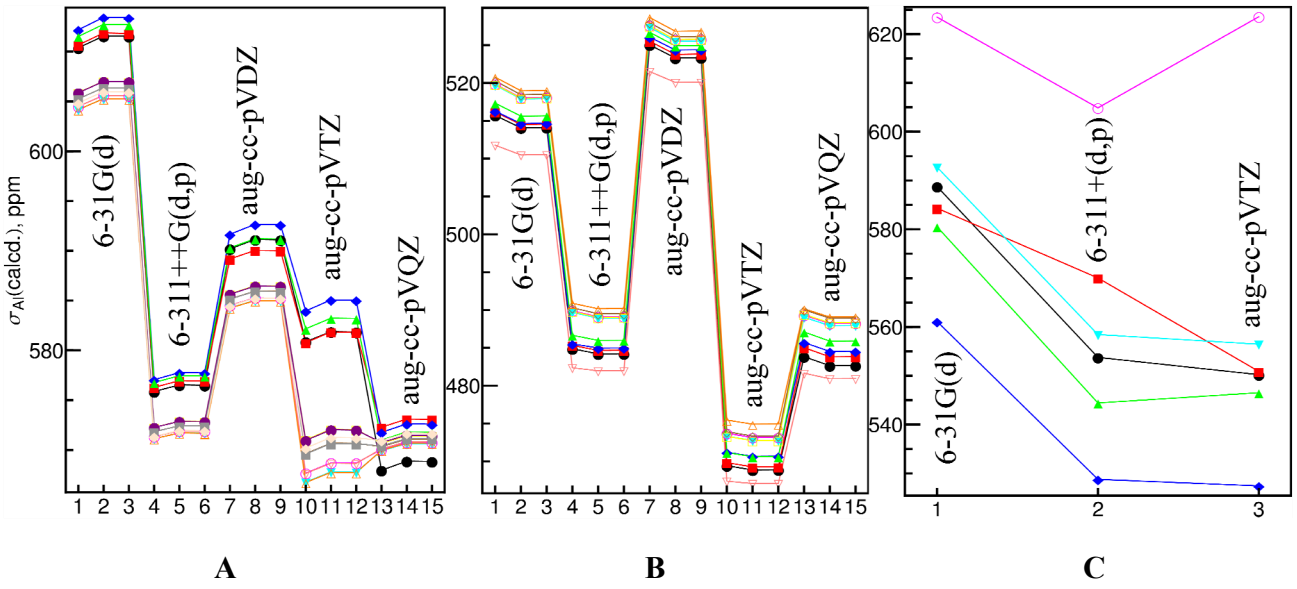

2.2. Comparison between Experimental and Calculated Chemical Shifts

From the previous subsection, we see that the shielding constants have a strong linear correlation among five levels of theory, though the absolute numbers differ from each other significantly. In practice, the chemical shifts are our primary concern, since the absolute chemical shielding constants are difficult to measure experimentally. Chemical shifts are related to shielding constants through the approximate equation, $\delta_{species} = \sigma_{ref} - \sigma_{species}$. ^{27}Al chemical shifts are usually referred to the aqueous $[Al(OH_2)_6]^{3+}$ species in acidic solutions. We use the averaged chemical shielding constant of the

$[Al(OH_2)_6]^{3+}$ species at the corresponding level to calculate the chemical shifts of other species. The results are given in Table 1.

Table 1. Comparison between the calculated and experimental ^{27}Al chemical shifts.

Species [a]	Refs.	^{27}Al chemical shifts				
		GIAO-B3LYP/6-31G(d) [b]	GIAO-B3LYP/6-311+G(d,p) [b]	GIAO-HF/6-311+G(d,p) [b]	GIAO-B3LYP/6-31G(d)//B3LYP/6-31G(d) [c]	Expt.[d]
Chemical shift reference						
$[Al(OH_2)_6]^{3+}$	[20–24]	0 ± 2.87	0 ± 3.44	0 ± 2.99	0	0
Al(III) hydrolysis products						
$[Al_2(\mu_2\text{-}OH)_2(OH_2)_8]^{4+}$	[25]	0.74 ± 1.94	1.73 ± 0.11	−1.30 ± 2.35	3.23	4.2
$[Al_8(\mu_3\text{-}OH)_2(\mu_2\text{-}OH)_{12}(OH_2)_{16}]^{10+}$	[26]	0.34 ± 0.39				4.8 (MAS)
		5.67 ± 0.11				8.4
		9.53 ± 0.10				11
$[AlO_4Al_{12}(\mu_2\text{-}OH)_{24}(OH_2)_{12}]^{7+}$ (Keggin-Al_{13})	[25]	52.95 ± 0.02	61.50 ± 0.52	57.30		63.5
		7.05 ± 0.53	6.53 ± 0.67	4.52 ± 0.65		12
$[Al_{13}(\mu_3\text{-}OH)_6(\mu_2\text{-}OH)_{12}(OH_2)_6]^{15+}$ (flat-Al_{13})	[27]	15.74				
		9.71 ± 0.79				
		0.25 ± 0.32				
$[Al_{30}(\mu_4\text{-}O)_8(\mu_3\text{-}OH)_6(\mu_2\text{-}OH)_{50}(OH_2)_{24}]^{15+}$ (Al_{30})	[25]	4.08 ± 1.18				4
		8.57 ± 0.41				5~12
		64.38 ± 0.51				64.5
Al(III) complexation with carboxylate and carbonyl groups						
$[AlL_6]^{3-}$, L = formate	[28]	0.92	−4.12	−2.56		
$[AlL_6]^{3+}$, L = dimethylformamide	[29,30]	3.20 ± 0.46	-0.78 ± 0.60	0.42 ± 0.41		
$[AlL_6]^{3+}$, L = dimethylacetamide	[31]	−6.97	-16.13	−15.50		
$[AlL_3]^{3-}$, L = oxalate	[32–39]	13.35 ± 0.97	14.77 ± 0.97	15.43 ± 1.12	20.15	16.3
$[AlL_2(OH_2)_2]^-$, L = malonate	[40]	4.81	4.32	3.65	19.77	2.5
$[AlL_2(OH_2)_2]^-$, L = methylmalonate	[21]	8.29	2.93	4.14		
$[AlL_3]^{3+}$, L = acetylacetone	[41–44]	2.44 ± 0.84	−2.29 ± 0.50	−0.40 ± 0.87		0.88
$[AlL_3]^{3+}$, L = 1,3-diphenylpropane-1,3-dione	[45]	7.39	−0.37	2.15		
$[AlL_3]^{3+}$, L = 1,3-dimesitylpropane-1,3-dione	[46]	5.26	−0.38	1.65		
$[AlL_3]^{3+}$, L = 1,3-bis(pentafluorophenyl)propane-1, 3-dione	[47]	2.39	−1.52	0.37		
$[AlL_3]^{3+}$, L = methylacetoacetate	[48]	6.54	2.60	2.60		
$[AlL_3]^{3+}$, L = *t*-butylacetoacetate	[49]	3.74	−0.91	−1.17		
$[AlL_3]^{3+}$, L = 3-(4-pyridyl)-2,4-pentanedione	[50]	2.17	−3.12	−0.40		
$[AlL_3]^{3+}$, L = 3-phenyl-2,4-pentanedione	[50]	2.53	−3	−0.51		
AlL_3, L = *iso*-maltol	[51]	5.98	1.22	1.37	12.60	2.9
Al(III) complexation with catechol-like ligands						
AlL_3, L = maltol	[52]	34.10 ± 0.17	39.04 ± 0.13	31.82 ± 0.12	43.36	37, 38
AlL_3, L = 2-ethylmaltol	[53]	33.86	38.80	31.48	43.74	38
$[AlL]^{3-}$, L = tris(*N*,*N*'-diethyl-2,3-dihydroxoterephthalamide)diamine	[54]	30.30	32.66	26.75		26

Table 1. *Cont.*

Species [a]	Refs.	^{27}Al chemical shifts				
		GIAO-B3LYP/6-31G(d) [b]	GIAO-B3LYP/6-311+G(d,p) [b]	GIAO-HF/6-311+G(d,p) [b]	GIAO-B3LYP/6-31G(d)//B3LYP/6-31G(d) [c]	Expt. [d]
AlL_3, L = 3-hydroxy-2-pyridone	[55]	24.09	33.43	27.05		
AlL_3, L = 1,2-dimethyl-3-hydroxy-4-pyridone	[56,57]	32.32 ± 0.00	37.04 ± 0.00	28.75 ± 0.00		36, 39
AlL_3, L = 1-*n*-propyl-2-methyl-3-hydroxy-4-pyridone	[58]	31.80	35.76	28.37		37
AlL_3, L = 1-*n*-butyl-2-methyl-3-hydroxy-4-pyridone	[58]	31.21	35.51	27.77		37
AlL_3, L = 1-*p*-tolyl-2-methyl-3-hydroxy-4-pyridone	[59]	33.74	38.55	30.39		37
AlL_3, L = tropolone	[60]	32.68	36.11	29.72	42.72	36.6
AlL_3, L = 6-*i*-propyltropolone	[61]	33.42	36.50	29.84		
Al_2L_3, L = 1,3-bis((3-oxy-1-methyl-2-oxo-1,2-dihydropyridin-4-yl)carboxamido)-2,2-dimethylpropane	[62]	28.67 ± 0.00	34.18 ± 0.00			
$[Al_2(\mu_2\text{-}O)_2\ L_4]^{4-}$, L =1,2-dihydroxyanthraquinone	[63]	23.01 ± 0.00				
$[Al_2(\mu_2\text{-}O)_2\ L_4]^{4-}$, L =1,2,4-trihydroxyanthraquinone	[64]	23.67 ± 0.05				23.1
Al(III) complexation with carboxylate and hydroxyl groups						
mer-$[AlL_3]^{3-}$, L = glycolate	[65]	30.86	37.08	28.13		
fac-$[AlL_3]^{3-}$, L = glycolate	[66]	27.65	31.59	23.55	34.00	25.5
$[AlL_3]^{3-}$, L = lacate	[67]	23.12 ± 0.13	26.32 ± 0.26	21.16 ± 0.16	33.44	24
$[AlL_2]^{5-}$, L = H_{-1}citrate	[68,69]	19.07 ± 0.45	18.04 ± 0.68	17.33 ± 0.71	25.69	21.4
$[Al_2L_3]^{6-}$, L = H_{-1}citrate	[70]	25.36	20.72	17.98		
		20.28	14.44	11.40		
$[Al_3L_3(\mu_2\text{-}OH)(OH_2)]^{4-}$, L = H_{-1}citrate	[71]	3.43	−0.44	0.05	20.74	0.6
		14.42	9.81	9.32	22.00	10.9
		15.90	9.81	8.41	23.00	12.9
$[Al_3L_2(\mu_2\text{-}OH)_2(OH_2)_4]^{-}$, L = H_{-1}citrate	[20]	5.43 ± 0.70				
		25.75				
$[Be_2Al_2L_4]^{6-}$, L = H_{-1}citrate	[72]	17.79 ± 0.87				14.0
$[Be_6Al_6L_6]^{18-}$, L = H_{-1}citrate	[72]	3.07 ± 0.18				12.2
$[Al_4L_6]^{6-}$, L = H_{-1}malate	[73]	23.27 ± 0.00	20.20 ± 0.00	15.83 ± 0.00		17.2
		6.35 ± 0.00	1.14 ± 0.00	1.18 ± 0.00		1.6
$[Al_4L_4(\mu_2\text{-}OH)_2]^{2-}$, L = H_{-1}malate	[73]	25.10 ± 0.79	28.46 ± 0.87	21.02 ± 1.06		2.2,1.6
		5.59 ± 1.02	1.83 ± 1.28	1.80 ± 1.11		1.1
$[Al_2L_2(OH_2)_2]^{2-}$, L = H_{-1}saccharate	[74]	28.61 ± 0.00	29.21 ± 0.00	24.36 ± 0.00	65.49	
$[Al_6L_4(\mu_2\text{-}OH)_8]^{6-}$, L = H_{-4}galactarate	[75]	16.43 ± 2.40	17.82 ± 1.13	11.64 ± 1.12		16.1, 16.8, 17.4, 17.7 (MAS)
		20.54 ± 1.74	21.27 ± 1.14	15.86 ± 1.75		22.6, 21.9 (MAS)
Al_2L_2(μ2-*t*-butoxo)2(*t*-butyoxy-*t*-butylperoxy), L = *o*-methoxycarbonyl phenoxy	[76,77]	11.91 ± 0.00	3.99 ± 0.00	3.94 ± 0.01		
		62.46 ± 0.00	61.47 ± 0.01	64.46 ± 0.01		
$[AlL_2L'_2]^{-}$, L = acetylacetonate, L' = *iso*-propoxo	[78]	9.25	2.89	4.44		
$Al_2L_4L'_2$, L = 3,5-heptanedionato, L' = *iso*-propoxo	[79]	9.69 ± 0.00	4.71 ± 0.00	2.40 ± 0.00		

Table 1. *Cont.*

Species [a]	Refs.	^{27}Al chemical shifts				
		GIAO-B3LYP/6-31G(d) [b]	GIAO-B3LYP/6-311+G(d,p) [b]	GIAO-HF/6-311+G(d,p) [b]	GIAO-B3LYP/6-31G(d)//B3LYP/6-31G(d) [c]	Expt. [d]
$[AlL]^+$, L = (2-hydroxybenzoyl-2-aminoethyl)-bis (2,3-dihydroxybenzoyl-2-aminoethyl)ammonio	[80]	8.05	1.26	3.95		
$[AlL]^+$, L = tris((2-Hydroxybenzoyl)-2-aminoethyl)ammine	[81]	7.04	0.38	2.64		
$[AlL]^+$, L = tris((2-Hydroxy-3-methoxybenzoyl)-2-aminoethyl)ammine	[81]	6.05	0.27	2.24		
Al(III) complexation with polyamino-polycarboxylates						
$[AlL]^-$, L = ethylenediaminetetraacetate	[82–84]	40.87 ± 2.57	42.22 ± 1.67	36.49 ± 1.27	47.88	41.2
$[AlL_2]^-$, L = iminodiacetate	[85–87]	37.94 ± 0.66	41.68 ± 0.60	35.15 ± 0.42	41.69	36.5
$[AlL_2]^-$, L = methyliminodiacetate	[88]	41.69 ± 0.62	43.18 ± 0.91	36.82 ± 0.63		
$Al_2L_2(\mu_2\text{-}OH)_2(OH_2)_2$, L = iminodiacetate	[86,89]	20.12 ± 0.67	22.07 ± 1.60	18.56 ± 1.03		
AlL, L = 1,4,7-triazacyclononane-N,N',N''-triacetate	[90,91]	52.17 ± 0.82	49.37 ± 1.44	44.68 ± 0.73		
$[AlL_2]^-$, L = dipicolinate	[92]	22.62	27.33	23.22		
$AlL(OH_2)_2$, L = nitrilotriacetate	[93]	24.77	25.74	21.60		
$[Al_2L_2(\mu_2\text{-}OH)_2]^{2-}$, L = nitrilotriacetate	[93]	27.42 ± 0.00	26.82 ± 0.00	22.16 ± 0.00	40.27	25.4
$Al_2L_2(OH)_2$, L = *N*-(2-oxyethyl)iminodiacetate	[94]	30.05 ± 0.00	28.59 ± 0.00	24.17 ± 0.00		32.8
$Al_2L_2(\mu_2\text{-}OH)_2$, L = ethylene-*N*,*N*'-bis(3-hydroxy propionato)	[95]	29.00 ± 1.69	27.50 ± 1.33	24.23 ± 1.41	38.74	25~30
$[Al_4L_2(\mu_2\text{-}OH)_4]^{2-}$, L = 1,3-diamino-2-propanolato-*N*,*N*,*N*',*N*'-tetraacetato	[86]	27.26 ± 1.69	25.83 ± 1.00	19.69 ± 0.56		
$[Al_4L_2L'_2(\mu_2\text{-}OH)(\mu_2\text{-}O)]^-$, L = *N*-(3-ammoniopropyl)carbamato, L' = 1,3-diamino-2-propanolato-*N*,*N*,*N*',*N*'-tetraacetato	[86]	30.00 ± 0.50	27.11 ± 1.36	22.54 ± 0.15		
Al(III) complexation with mixed O and N ligands						
AlL_3, L = 8-hydroxyquinoline	[96–100]	30.68 ± 1.84	31.27 ± 1.37	29.39 ± 1.68	40.41	31.1
AlL_3, L = 2-methyl-8-hydroxyquinoline	[101]	33.28	35.11	31.33		
AlL_2L', L = 2-methyl-8-hydroxyquinoline, L' = picolinato	[102]	28.81	29.78	26.97		
$Al_2L_4(\mu_2\text{-}2\text{-}(ethoxy)ethoxo))_2$, L = 8-hydroxyquinoline	[103]	28.14 ± 0.44	24.82 ± 1.21	22.39 ± 1.29	37.52	26.9
Al_2L_3, L = 1,3-bis(8-hydroxyquinolin-7-yl)-2-methylene-propane	[104]	33.55 ± 0.00	34.88 ± 0.00	31.92 ± 0.00		
AlL_3, L = 2-(2-hydroxyphenyl)-5-phenyl-1,3,4-oxadiazole	[105]	8.95	−0.96	3.41		
$[AlL_2]^-$, L = 1-phenyl-3,5-bis(2-oxyphenyl)-1,2,4-triazole	[106]	6.91	0.85	2.80		
$[AlL_2(OH_2)_2]^+$, L = *N*,*N*'-bis(3,5-*di*-*t*-butylsalicylidene)ethylenediamine	[107]	7.41	5.02	8.07		
$[AlL_2(CH_3OH)_2]^+$, L = *N*,*N*'-bis(3,5-*di*-*t*-butylsalicylidene)ethylenediamine	[107]	11.62 ± 1.47	8.59 ± 2.08	9.40 ± 1.21		
$[AlL_2(OH_2)_2]^-$, L = 1,9-bis(2-oxyphenyl)-5-phenyldipyrrine	[108]	6.67	3.16	5.88		
$AlLL'_2$, L = 5,10,15,20-tetraphenylporphyrine, L' = tetrahydrofuran	[109]	−5.41	−15.23	−10.73		

Table 1. *Cont.*

Species [a]	Refs.	^{27}Al chemical shifts				
		GIAO-B3LYP/6-31G(d) [b]	GIAO-B3LYP/6-311+G(d,p) [b]	GIAO-HF/6-311+G(d,p) [b]	GIAO-B3LYP/6-31G(d)//B3LYP/6-31G(d) [c]	Expt. [d]
AlL_2, L = 3,5-*di*-*t*-butyl-1,2-quinone-1-(2-hydroxy-3,5-*di*-*t*-butylphenyl)imine	[110]	50.61	50.41	41.14		
$AlL_2L'_2$, L =2,2,6,6-tetramethylheptane-3,5-dionato, L' = 2-((2-hydroxy)benzylidene)amino)phenolato	[111]	12.17 ± 0.00	7.15 ± 0.00	6.82 ± 0.00		
$Al_2L_4(\mu_2\text{-}OH)_2$, L = 2-(2-oxyphenyl)benzimidazole	[112]	7.96 ± 0.00	1.56 ± 0.00	2.80 ± 0.00		
$Al_2L_4(\mu_2\text{-}OH)_2$, L = 2-(2'-hydroxyphenyl)-2-benzoxazolato	[113]	14.92 ± 0.21	± 0.00	8.12 ± 0.05		5
$[AlL_2]^-$, L = nordesferriferrithiocin	[114]	19.95	17.46	16.86		
$[AlL_2]^-$, L = desferriferrithiocin	[114]	12.84	4.89	7.58		
AlL, L = alumichrome A	[115]	26.96				31.54
$[AlL]^+$, L =tris(5'-chloro-2'-hydroxybenzylaminoethyl)amine	[116]	19.87	11.25	13.95		
$[Al_3(\mu_3\text{-}O)L_6L'_3]^+$, L = acetate, L' = acetonitrile	[116]	2.66 ± 0.24	−1.08 ± 0.17	−0.16 ± 0.57		
Al(III) complexation with N's						
$[AlL_6]^{3+}$, L = acetonitrile	[118]	−20.44 ± 2.21	−37.13 ± 1.12	−27.74 ± 1.59	−14.60	−33
AlL_3, L = bis(2-pyridyl)amido	[119]	28.36	20.50	23.19		
AlL_3, L = 1,3-bis(2-methylphenyl)triazenido	[120]	28.62	16.35	21.86	41.93	28
AlL_3, L = 1,3-bis(4-chlorophenyl)triazenido	[120]	28.62	23.05	23.15		26
AlL_3, L = 1,3-bis(4-methoxyphenyl)triazenido	[120]	26.60	20.75	21.82	41.48	27
AlL_3, L = 1,3-diphenyltriazenido	[121]	26.72	21.26	21.82		25
Al(III) complexation with P and other ligands						
$[Al(H_2L)_3(HL)_3]^{6-}$, L = phosphate	[122]	−9.22	10.78	−14.88		−15.2
$[Al_4(HL)_4L'_{12}]^{4+}$, L = phosphate, L' = ethanol	[123]	1.32 ± 0.00 1.77 ± 0.00				−8.7, −8.8 (MAS) −8.2
$[Al_2L_2L'_8]^{4+}$, L = phenylphosphinato, L' = *n*-butanol	[124]	4.91 ± 0.00	2.04 ± 0.00	0.09 ± 0.00		−2.5
$[Al_3L_2L'_{10}(\mu_2\text{-}OH)]^{4+}$, L = phenylphosphinato, L' = ethanol	[125]	−0.02 3.42 ± 0.69				−2.2 1.5
$[Al_5L_4L'_{10}(\mu_2\text{-}OH)_2]^{5+}$, L = phenylphosphinato, L' = *sec*-butanol	[126]	−0.32 ± 0.07 40.99				0 48.7
Al(III)-fluoride complexes						
$[AlF_6]^{3-}$	[127–132]	17.60 ± 0.84	−1.05 ± 0.88	−4.77 ± 1.22		−5, −0.1, −0.6, −2.4, −2.7, −2.8, −17.9,
$[AlF_5(OH_2)]^{2-}$	[129, 133–135]	17.46 ± 1.26	5.18 ± 1.46	−0.05 ± 2.33		−6.3, −12.0, −13.8, −14.4
$[Al_2F_{10}]^{4-}$	[136,137]	18.35 ± 0.97				
$[Al_4F_{18}]^{6-}$	[129]	12.62 ± 0.06				
$[Al_7F_{30}]^{9-}$	[138]	−3.59 12.16 ± 0.29				
$[AlF_2L_4]^+$, L = pyridine	[139]	6.74 ± 0.47	2.10 ± 1.75	4.19 ± 0.04	13.53	3.6 (MAS)

Table 1. *Cont.*

Species [a]	Refs.	^{27}Al chemical shifts				
		GIAO-B3LYP/6-31G(d) [b]	GIAO-B3LYP/6-311+G(d,p) [b]	GIAO-HF/6-311+G(d,p) [b]	GIAO-B3LYP/6-31G(d)//B3LYP/6-31G(d) [c]	Expt. [d]
Tetrahedral-coordinated Al(III) with O's						
$[Al(OR)_4]^-$, R = $C(CF_3)_3$	[140–143]	40.55	33.09	38.36	51.71	38.8
		41.41	33.35	38.80		36.2
		39.71	32.22	36.79		37.5
		36.58				
		35.84	26.16	32.88		36
		41.08	29.83	38.56		33.8
		31.80	21.82	27.67		34.1
		39.66	31.83	36.86		34.1
		41.91		39.54		
$[Al(OR)_4]^-$, R = $CH(CF_3)_2$	[142,144]	58.23 ± 0.33	56.30 ± 0.11	58.42 ± 0.64	69.97	58
		61.18	60.69	61.91		58
		55.61	52.74	54.95		56.9
$[Al(OR)_4]^-$, R = $C(CH_3)(CF_3)_2$	[142,144]	50.29	45.58	49.88		45.2
		50.71	44.95	49.34		45.6
$[(OR)_3Al\ FAl(OR)_3]^-$, R = $C(CF_3)_3$	[141]	32.62 ± 1.47	27.89 ± 1.89	33.22 ± 2.21	46.30	36
Tetrahedral-coordinated Al(III) with C's and N's						
$Al_2L_2L'_4$, L = pyrazolyl, L' = *t*-butyl	[145]	143.64 ± 0.00	146.56 ± 0.00	148.74 ± 0.00	143.42	150
$Al_2L_2L'_4$, L = 3,5-dimethylpyrazolyl, L' = methyl	[77]	140.62 ± 0.00	164.46 ± 0.00	158.22 ± 0.00	139.69	150
$AlLL'_2$, L = 1,3-diphenyltriazenido, L' = *iso*-butyl	[120]	170.36	189.01	178.95		
$AlLL'_2$, L = 1,3-diphenyltriazenido, L' = 2,6-di-*t*-butyl-4-methylphenoxy	[120]	41.52	44.09	50.88	45.65	31
Penta-coordinated Al(III) complexes						
$[AlL]^{2-}$, L = (2-hydroxy-3-methoxybenzoyl-2-aminoethyl)-bis(2,3-dihydroxybenzoyl-2-aminoethyl)amine	[79]	51.30	53.08			
$[AlL]^{2-}$, L = (2-hydroxybenzoyl-2-aminoethyl)-bis(2,3-dihydroxybenzoyl-2-aminoethyl)amine	[79]	56.30				
AlLL', L = *N*,*N*'-ethylene-bis(salicylideneamino-), L' = methyl	[119]	61.12	66.86	64.69		
$B_2Al_2(\mu_2\text{-ethoxo})L_4L'_6$, L = pyrazolyl, L' = ethyl	[77]	67.85 ± 0.00	68.09 ± 0.00	66.20 ± 0.00	72.01	62

[a] "H_{-1}" in the complexation species refers that the hydroxyl group or one of the hydroxyl groups in the ligand is deprotonated; [b] The chemical shifts were obtained by subtracting the calculated isotropic chemical shielding constants from the averaged isotropic shielding tensor of the reference species computed at the same theoretical level. The calculated ^{27}Al chemical tensors were obtained with the GIAO method at three theoretical levels: B3LYP/6-31G(d), B3LYP/6-311+G(d,p) and HF/6-311+G(d,p) and the X-ray crystallographic structures were used for the molecular geometries. The values following "±" are the standard deviations of the calculated values of either several models or multiple chemically equivalent sites; [c] The molecular geometries were optimized at the B3LYP/6-31G(d) level, followed by a chemical shielding tensor calculation at the GIAO-B3LYP/6-31G(d) level; [d] The values followed by "(MAS)" refer that the measurements were done using the solid-state MAS ^{27}Al NMR spectroscopy and the isotropic chemical shifts were obtained by a fitting procedure from the spectra. Otherwise, the measurements were done in the solution state.

How do these models perform when compared with the experimental measurements? We searched the literature for experimental ^{27}Al NMR studies of Al(III) species and picked the species whose ^{27}Al chemical shifts were assigned. The measurements include both solution-state and solid-state magic-angle-spin (MAS) ^{27}Al NMR spectra. For the latter, the isotropic chemical shifts were calculated by fitting the simulated spectra with the experimental spectra. The solution-state NMR measurements were for the Al(III) species in both aqueous and organic solvents. Therefore, the experimental chemical shifts are measured at a wide range of different chemical environments. But the calculations were done for the isolated molecules. How strongly are the ^{27}Al chemical shifts dependent on the long-range chemical environment? The answer might be different for different species, but the environment effect might be small for most Al(III) species because the first coordination layer dominates the shielding effect to the ^{27}Al nucleus. For example, the chemical shifts of the tetrahedral-coordinated $[Al(OC(CF_3)_3)_4]^-$ with various kinds of counter ions in different solvents, range from 38.8 to 33.8 ppm [140–143]. On the other hand, the chemical environment has a significant effect on the small $[AlF_6]^{3-}$ species and fast ligand exchange occurs in aqueous solutions [148,149]. The solid-state MAS NMR studies found the isotropic chemical shifts of $[AlF_6]^{3-}$ range from −0.1 to −17.9 ppm for which the counter ions include H^+, K^+, NH_4^+ and Rb^+ [150]. The values for $[AlF_5(OH_2)]^{2-}$ obtained from the solid-state MAS NMR spectra range from −6.3 to −14.4 ppm [150]. These results reflect the sensitivity of chemical shifts of small size species to chemical environment. The environment could affect the ^{27}Al chemical shifts through two aspects. The first is that the geometry parameters, such as bond lengths and bond angles, of the first coordination layer could be perturbed by the packing forces, by the electrical field and/or by solvation. The other factor is that the chemical environment other than the first coordination layer could contribute to the shielding or to the deshielding effect to the metal center. For the isolated molecule models used to compute the chemical shieldings, counter ions and solvents were not included. Therefore, only the first effect was accounted for in the calculations.

The calculated chemical shifts *vs.* the experimental chemical shifts are shown in Figure 3. Black squares are the calculated shifts at the GIAO-B3LYP/6-31G(d) level, and red circles and blue triangles are the calculated values at GIAO-B3LYP/6-311+G(d,p) and GIAO-HF/6-311+G(d,p), respectively.

Comparing the calculated chemical shifts at the GIAO-B3LYP/6-31G(d) level with the experimental values, the absolute errors for most species are less than 12 ppm except for three outliers. About one third (31%) of the absolute errors are less than 2 ppm, while more than 79% in total are less than 6 ppm. The overall root-mean-square difference (RMSD) is 6.5 ppm. If the three outliers whose absolute errors are larger than 12 ppm are removed, the RMSD decreases to 4.4 ppm. From this result, we see that the popular GIAO-B3LYP model with the 6-31G(d) basis set performs quite well for predicting the ^{27}Al chemical shifts using the X-ray measured geometries.

The three outliers are $[AlF_6]^{3-}$, $[Al(NCCH_3)_6]^{3+}$ and $[Al_4(\mu_2\text{-}OH)_2(\mu_2\text{-}H_{-1}malato)_4]^{2-}$. In calculating δ_{Al} for $[AlF_6]^3$ the large error is probably due to its small size [150]. Calculations including the ion's environment beyond the binding ligands would probably significantly improve the result. For the acetonitrile complex, the ligand is disordered in the crystals and not accounting for the distribution in geometries might lead to a significant error [118]. For the polymeric malate complex, the ^{27}Al NMR spectra are not well defined, so there might be a significant error associated with the experimental determination of δ_{Al} [73].

Figure 3. Correlation between the experimental ^{27}Al chemical shifts *versus* the calculated values using the X-ray crystallographic geometries at the GIAO-B3LYP/6-31G(d) (black squares), the B3LYP/6-311+G(d,p) (red circles) and the HF/6-311+G(d,p) (blue triangles) levels. The black solid line, the red dashed line and the dotted blue lines are the best-fit linear regression of the three data sets, respectively, and the best-fit equations are given in Equations 3–5.

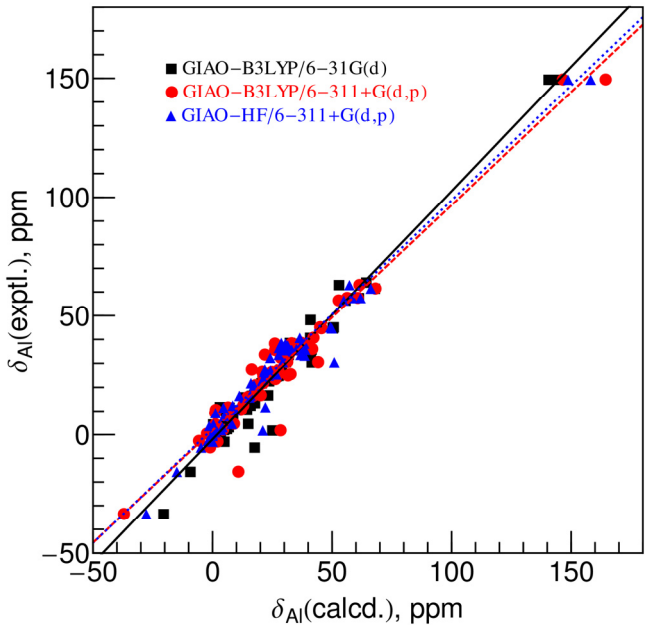

$$\delta_{Al}\text{ (GIAO-B3LYP/6-31G(d))} = -1.18 + 1.03\ \delta_{Al}(\text{expt}),\ R^2 = 0.94 \quad (3)$$

$$\delta_{Al}\text{ (GIAO-B3LYP/6-311+G(d,p))} = 1.67 + 0.95\ \delta_{Al}(\text{expt}),\ R^2 = 0.94 \quad (4)$$

$$\delta_{Al}\text{ (GIAO-HF/6-311+G(d,p))} = 2.63 + 0.96\ \delta_{Al}(\text{expt}),\ R^2 = 0.96 \quad (5)$$

When the larger basis set, 6-311+G(d,p), is used, the accuracy improves slightly. The RMSD between the calculated chemical shifts at the GIAO-B3LYP/6-311+G(d,p) level and the experimental values for all the species is 6.6 ppm and it decreases to 3.9 ppm after removing the three outliers whose absolute errors are larger than 12 ppm. About 40% of the absolute errors are less than 2 ppm, while 80% in total are less than 6 ppm.

The accuracy of the chemical shifts calculated at the GIAO-HF/6-311+G(d,p) level is slightly worse than that of the GIAO-B3LYP/6-31G(d) level. Although the RMSD for all the data points is 5.7 ppm which is less than the other two models, it decreases to 4.8 ppm after removing two outliers whose absolute errors are larger than 12 ppm. One third (33%) of the absolute errors are less than 2 ppm and 72% in total are less than 6 ppm.

By comparing the results of the three levels of theory, we see that they are similar in terms of the capability in predicting the ^{27}Al chemical shifts, though the GIAO-B3LYP/6-311+G(d,p) model is slightly better than the other two.

As seen from Figure 3, the calculated chemical shifts at three levels were well correlated with the experimental results, except for a few outliers. The best-fit equations are given in Equations 3~5 for the correlation between the calculated chemical shifts at the GIAO-B3LYP/6-31G(d),

GIAO-B3LYP/6-311+G(d,p) and GIAO-HF/6-311+G(d,p) levels, respectively, *versus* the experimental values (black solid line, red dashed line and blue dotted line, respectively in Figure 3).

2.3. Geometry Optimization

In a practical application scenario, the structure of the proposed complex is unknown. Geometry optimization is used to obtain the structure in the first place. Does the error of the calculated geometries contribute significantly to an error in predicting ^{27}Al chemical shifts? To investigate this question, the experimental geometries of 33 complexes were optimized at the B3LYP/6-31G(d) level, followed by a shielding tensor calculation using the GIAO-B3LYP/6-31G(d) model.

The calculated δ_{Al} are plotted against the experimental values in Figure 4. On one hand, the calculated δ_{Al} are systematically larger than the experimental values; on the other hand, the slope of the best-fit equation which is given in Equation 6 and plotted as the black line in Figure 4 is 1.10. The 95% confidence interval for the slope is 1.04 to 1.17. The systematic larger calculated chemical shifts may be because the shielding constant of the reference $[Al(OH_2)_6]^{3+}$ species is overestimated in the optimized geometry. The calculated σ_{Al} in the optimized geometry is 16.7 ppm larger than that in the X-ray geometry, which reflects the elongation of Al–O bonds by 0.06 Å in the optimized geometry compared with the mean value in the X-ray geometry. The latter deviation reflects that the single-molecule calculated geometry at the B3LYP/6-31G(d) level causes significant errors in predicting δ_{Al}. Until such time as experimental techniques can unequivocally determine structures of molecules in liquid solvents, this issue cannot be unambiguously settled.

Figure 4. Correlation between the experimental ^{27}Al chemical shifts *versus* the calculated values at the GIAO-B3LYP/6-31G(d) level using the optimized geometries at the B3LYP/6-31G(d) level. The black solid line is the best-fit linear regression of the data and the best-fit equation is given in Equation 6, while the dashed red line is the ideal diagonal line ($y = x$).

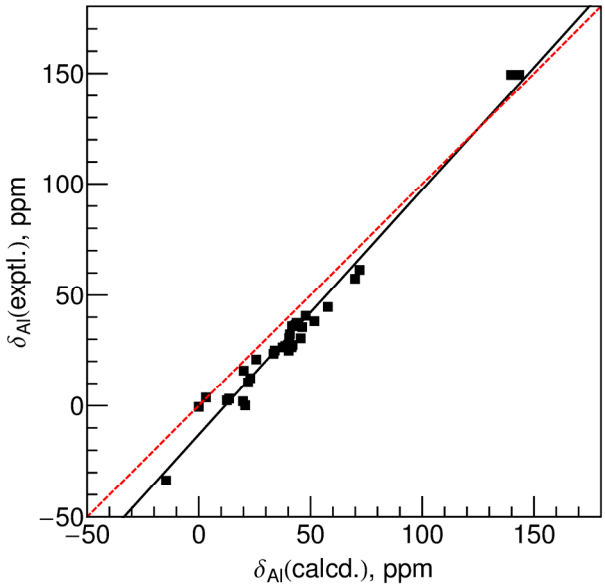

$$\delta_{Al}\ (\text{GIAO-B3LYP/6-31G(d)//B3LYP/6-31G(d)}) = -13.0 + 1.10\ \delta_{Al}\ (\text{expt}),\ R^2 = 0.97 \quad (6)$$

The RMSD for all the data points is 10.9 ppm. Even after removing the points with errors larger than 12 ppm, the RMSD is about 8.4 ppm. If we offset all the calculated δ_{Al} by 15.4 ppm, *i.e.* to let the best-fit equation cross the origin point, the calculated RMSD is still as large as 7.7 ppm. Therefore, an accurate geometry is critical in calculating ^{27}Al chemical shifts.

2.4. Solvent Effect

Solvent effect plays an important role in solution-state ^{27}Al NMR. Without the constraint of the periodic boundary condition in the crystals, the geometries will be slightly different, the long-range interactions will be dramatically different and dynamical effect will be also different. In this study, we only examined how the commonly used implicit solvation model affects the prediction of ^{27}Al chemical shifts. The self-consistent reaction field (SCRF) method [151] with the polarizable continuum model (PCM) [152] of water and/or methanol was applied to the calculation of the shielding constants and the geometry optimization. In Figure 2, we have seen that the calculated shielding constants of $[Al(OH_2)_6]^{3+}$ and $[Al(OH)_4]^-$ in the PCM environment of water or methanol are nearly the same as those obtained in vacuum using the same geometry. However, the calculated shielding constants using the geometries optimized in the PCM environment of water or methanol differ by 5~10 ppm from those obtained with the optimized geometries in vacuum. The differences in $[Al(OH_2)_6]^{3+}$ are larger than those in $[Al(OH)_4]^-$, which reflects the former species is more sensitive to the solvation effect. At the B3LYP/aug-cc-pVQZ level, the calculated Al–O bond length of $[Al(OH_2)_6]^{3+}$ in water or methanol is 0.036 Å shorter than that obtained in vacuum in average (1.896 Å *vs.* 1.932 Å), while the difference is only 0.008 Å in $[Al(OH)_4]^-$ (1.770 Å *vs.* 1.778 Å).

Two more groups of calculations were carried out on 10 representative complexes. In the first group of calculations, the influence of the PCM model to the calculation of the shielding constants was examined using the X-ray geometries at the GIAO-B3LYP/6-31G(d) level. In the second group of calculations, both the geometry optimization and the shielding constants calculation were carried out in the PCM environment of water at the B3LYP/6-31G(d) level. The calculated σ_{Al} values were compared with the values obtained in vacuum using the X-ray geometries. The differences are plotted in Figure 5, where the blue and red bars are for the first and second groups of calculations, respectively. Again, we see that the PCM model only causes a minor change to the calculated σ_{Al} if the same geometry was used. However, if the geometry optimization was applied, significant changes were observed. This result again says that the geometry parameters of the complexes have a big influence on the calculated σ_{Al}.

3. Computational Details

The crystal structures of 114 Al(III) complexes, determined by single-crystal X-ray diffraction, were obtained from the Cambridge Crystal Structural Database (Cambridge Crystallographic Data Centre, Cambridge, UK). They were used to build the molecular structures of the species. If there was more than one Al(III) species in the asymmetric unit, a molecular structure was built for each structure. For the disordered crystal structures, only the structure with major population was used to build the molecular model. In total, 213 molecular models were created from 206 crystal structures for 114 species. 33 complexes of small to intermediate sizes were optimized using the X-ray structures as the starting point.

Figure 5. Difference between the calculated σ_{Al} for 10 Al(III) complexes. The blue bars are the differences between the values in the PCM environment of water and in vacuum using the X-ray geometries. The red bars are the differences between the values calculated using the geometries optimized at the B3LYP/6-31G(d) level in the PCM environment of water and those calculated using the X-ray geometries in vacuum. All the σ_{Al} are calculated at the GIAO-B3LYP/6-31G(d) level. The complexes are $[Al(OH_2)_6]^{3+}$, $[Al(oxalate)_3]^{3-}$, $[AlF_6]^{3-}$, Al(8-hydroxyquinoline)$_3$, $[Al(EDTA)]^-$, Al(lactate)$_3$, $[Al(malonate)_2(OH_2)_2]^-$, $[Al(H_{-1}citrate)_2]^{5-}$, $[Al(N{\equiv}CCH_3)_6]^{3+}$ and Al(maltol)$_3$ for 1–10, respectively.

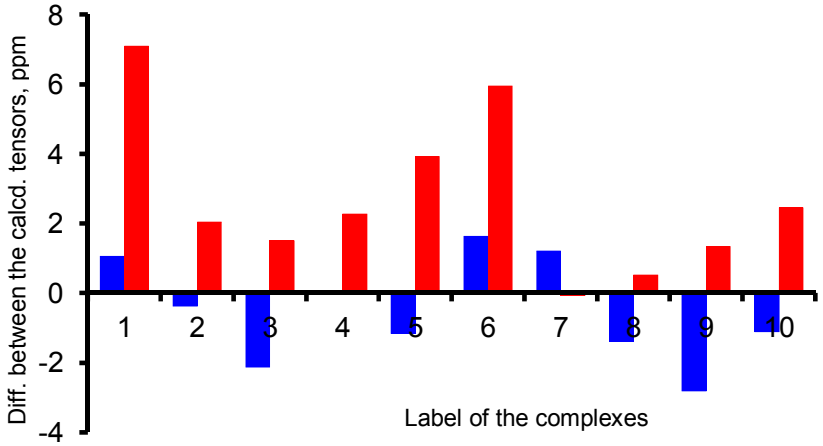

Only a single molecule was included in each molecular model. Hydrogen positions were put in their ideal positions with the aid of GaussView 3.0 (Gaussian, Inc., Wallingford, CT, USA) if they were missing from the crystal structures. All the counter ions and solvent molecules were excluded from the models. Chemical shielding tensors were calculated for these X-ray geometry models and the models with further geometry optimization at the B3LYP/6-31G(d) level.

All electronic structure calculations were done with the Gaussian03 program suite [153]. Chemical shielding tensors were calculated with the gauge-invariant atomic orbital (GIAO) formalism [5,6] of three theory models, Hartree-Fock, Becke-Lee-Yang three-parameter hybrid density functional theory (B3LYP) [154–157] and Møller-Plesset second-order perturbation theory (MP2) [158], with a series of basis sets, 6-31G(d) [159], 6-311+G(d,p) and 6-311++G(d,p) [160] and aug-cc-pV*X*Z (*X* = D, T and Q) [146,147]. The implicit solvent model of water and methanol was calculated using the self-consistent reaction field (SCRF) method [151] with the polarizable continuum model (PCM) [152]. ^{27}Al chemical shifts were obtained by subtracting the isotropic chemical shielding constants from the mean chemical shielding constant of the reference species, $[Al(OH_2)_6]^{3+}$, calculated at the same theory level.

4. Conclusions

The main purpose of this work is to give a quantitative evaluation of the errors involved in the calculation of ^{27}Al chemical shifts. We differentiated the source of the errors due to the limitations of the computational models in calculating the chemical shielding tensors and the inaccuracy in geometry prediction by using the X-ray measured geometries and the calculated geometries to compute chemical shifts. The RMSD between the calculated shifts and the experimental values is approximately 5 ppm if

the X-ray crystallographic structures were used, while the RMSD is more than 10 ppm for the optimized geometries at the B3LYP/6-31G(d) level. Although we could not isolate the error due to the structural uncertainties in the X-ray crystallography, the popular GIAO-B3LYP/6-31G(d) model produces quite accurate chemical shifts.

There are other error sources not considered in this study, such as the quality of DFT functionals and dynamical effects [161]. In addition, the structure of a complex in solution would be different from its crystal structure; the solvent effect is also more complicated than what has been studied here. However, the results presented in this study shows that the error associated with the shielding constants calculation is small compared with the error in the prediction of geometry. In particular, Jensen showed that the error in the shielding constants calculation can be controlled to less than 1 ppm. In the future, we should focus on predicting a more accurate geometry in solution or an ensemble of structural configurations generated using molecular dynamics.

Acknowledgments

The authors acknowledge the financial support from the National Natural Science Foundation of China (21103016) and the Research Fund for the Doctoral Program of Higher Education of China (20100185120023). We thank four anonymous reviewers for their insightful and constructive comments of our manuscript. We thank Peter Beckmann for English editing and proofreading of the manuscript.

Conflict of Interest

The authors declare no conflict of interest.

References

1. Lewis, T. *Environmental Chemistry and Toxicology of Aluminium*, 1st ed.; CRC Press: Boca Raton, FL, USA, 1989.
2. Sposito, G. *The Environmental Chemistry of Aluminum*, 2nd ed.; CRC Press: Boca Raton, FL, USA, 1995.
3. Wang, X.L.; Zou, G.; Bi, S. Advances in determination of aluminum in environmental and biological materials by ^{27}Al nuclear magnetic resonance spectroscopy. *Chin. J. Inorg. Chem.* **2000**, *16*, 548–560.
4. Tossell, J.A. The effects of hydrolysis and oligomerization upon the NMR shieldings of Be^{+2} and Al^{+3} species in aqueous solution. *J. Magn. Reson.* **1998**, *135*, 203–207.
5. Ditchfield, R. Self-consistent perturbation theory of diamagnetism. *Mol. Phys.* **1974**, *27*, 789–807.
6. Wolinski, K.; Hinton, J.F.; Pulay, P. Efficient implementation of the gauge-independent atomic orbital method for NMR chemical shift calculations. *J. Am. Chem. Soc.* **1990**, *112*, 8251–8260.
7. Amini, S.K.; Tafazzoli, M. DFT calculations as a powerful technique to probe the crystal structure of $Al(acac)_3$. *Magn. Reson. Chem.* **2008**, *46*, 1045–1050.

8. Schurko, R.W.; Wasylishen, R.E.; Foerster, H. Characterization of anisotropic aluminum magnetic shielding tensors. Distorted octahedral complexes and linear molecules. *J. Phys. Chem. A* **1998**, *102*, 9750–9760.
9. Mirzaei, M.; Mirzaei, M. Aluminum phosphide nanotubes: Density functional calculations of aluminum-27 and phosphorus-31 chemical shielding parameters. *J. Mol. Struct.* **2010**, *951*, 69–71.
10. Bodaghi, A.; Mirzaei, M.; Seif, A.; Giahi, M. A computational NMR study on zigzag aluminum nitride nanotubes. *Physica E* **2008**, *41*, 209–212.
11. Charpentier, T. The PAW/GIPAW approach for computing NMR parameters: A new dimension added to NMR study of solids. *Solid State Nucl. Magn. Reson.* **2011**, *40*, 1–20.
12. Pickard, C.J.; Mauri, F. All-electron magnetic response with pseudopotentials: NMR chemical shifts. *Phys. Rev. B* **2001**, *63*, 245101.
13. Pedone, A.; Gambuzzi, E.; Malavasi, G.; Menziani, M.C. First-principles simulations of the ^{27}Al and ^{17}O solid-state NMR spectra of the $CaAl_2Si_3O_{10}$ glass. *Theor. Chem. Acc.* **2012**, *131*, 1147.
14. Choi, M.; Matsunaga, K.; Oba, F.; Tanaka, I. ^{27}Al NMR chemical shifts in oxide crystals: A first-principles study. *J. Phys. Chem. C* **2009**, *113*, 3869–3873.
15. Mulder, F.A.; Filatov, M. NMR chemical shift data and *ab initio* shielding calculations: Emerging tools for protein structure determination. *Chem. Soc. Rev.* **2010**, *39*, 578–590.
16. Jensen, F. Basis set convergence of nuclear magnetic shielding constants calculated by density functional methods. *J. Chem. Theory Comput.* **2008**, *4*, 719–727.
17. Kubicki, J.D.; Sykes, D.; Apitz, S.E. *Ab initio* calculation of aqueous aluminum and aluminum-carboxylate complex energetics and ^{27}Al NMR chemical shifts. *J. Phys. Chem. A* **1999**, *103*, 903–915.
18. Qian, Z.; Feng, H.; He, L.; Yang, W.; Bi, S. Assessment of the accuracy of theoretical methods for calculating ^{27}Al nuclear magnetic resonance shielding tensors of aquated aluminum species. *J. Phys. Chem. A* **2009**, *113*, 5138–5143.
19. Stack, A.G.; Rustad, J.R.; Casey, W.H. Modeling water exchange on an aluminum polyoxocation. *J. Phys. Chem. B* **2005**, *109*, 23771–23775.
20. Malone, S.A.; Cooper, P.; Heath, S.L. Synthesis and structure of a new aluminium citrate trimer from aqueous solution at very low pH. *Dalton Trans.* **2003**, 4572–4573.
21. Karlsson, M.; Boström, D.; Öhman, L. Equilibrium and structural studies of silicon(IV) and aluminium(III) in aqueous solution. 33. The Al(methylmalonate)$_2$(H$_2$O)$^{2-}$ complex crystallised as a double salt with $Al(H_2O)_6^{(3+)}$ and Cl^-. *Acta Chem. Scand.* **1998**, *52*, 995–999.
22. Bataille, T. Hemi(piperazinediium) hexaaquaaluminium(III) bis(sulfate) tetrahydrate: A new double aluminium sulfate salt. *Acta Cryst. C* **2003**, *59*, m459–m461.
23. Dalrymple, S.A.; Parvez, M.; Shimizu, G.K. Intra- and intermolecular second-sphere coordination chemistry: Formation of capsules, half-capsules, and extended structures with hexaaquo- and hexaamminemetal ions. *Inorg. Chem.* **2002**, *41*, 6986–6996.
24. Shen, R.; Pan, X.; Wang, H.; Yao, L.; Wu, J.; Tang, N. Selective colorimetric and fluorescent detection of HSO_4^- with sodium(i), magnesium(ii) and aluminium(iii) xanthone-crown ether complexes. *Dalton Trans.* **2008**, 3574–3581.

25. Mainicheva, E.; Gerasko, O.; Sheludyakova, L.; Naumov, D.; Naumova, M.; Fedin, V. Synthesis and crystal structures of supramolecular compounds of polynuclear aluminum(III) aqua hydroxo complexes with cucurbit[6]uril. *Russ. Chem. Bull.* **2006**, *55*, 267–275.
26. Casey, W.H.; Olmstead, M.M.; Phillips, B.L. A new aluminum hydroxide octamer, $[Al_8(OH)_{14}(H_2O)_{18}](SO_4)_5 \cdot 16H_2O$. *Inorg. Chem.* **2005**, *44*, 4888–4890.
27. Gatlin, J.T.; Mensinger, Z.L.; Zakharov, L.N.; MacInnes, D.; Johnson, D.W. Facile synthesis of the tridecameric Al_{13} nanocluster $Al_{13}(\mu_3\text{-}OH)_6(\mu_2\text{-}OH)_{18}(H_2O)_{24}(NO_3)_{15}$. *Inorg. Chem.* **2008**, *47*, 1267–1269.
28. Plutecka, A.; Rychlewska, U. A three-dimensional Al^{III}/Na^{I} metal-organic framework resulting from dimethylformamide hydrolysis. *Acta Cryst. C* **2009**, *65*, m75–m77.
29. Bekaert, A.; Barberan, O.; Kaloun, E.B.; Rabhi, C.; Danan, A.; Brion, J.D.; Lemoine, P.; Viossat, B. Crystal structure of hexakis (*N*,*N*-dimethylformamide-*O*) aluminium (III) tris (tribromide), Al $[(CH_3)_2N(CH)O]_6(Br_3)_3$. *Z. Kristallogr.* **2002**, *217*, 128–130.
30. Suzuki, H.; Ishiguro, S. *N*,*N*-Dimethylformamide complex of aluminium(III) perchlorate. *Acta Cryst. C* **1998**, *54*, 586–588.
31. Suzuki, H.; Ishiguro, S. *N*,*N*-Dimethyl-acetamide complex of aluminium(III) perchlorate. *Acta Cryst. E* **2006**, *62*, m576–m578.
32. Riesen, H.; Rae, A.D. Revisiting the crystal structure and thermal properties of $NaMgAl(oxalate)_3.9H_2O$/Cr(iii): An extraordinary spectral hole-burning material. *Dalton Trans.* **2008**, 4717–4722.
33. Taylor, D. Crystal structures of potassium tris(oxalato) chromate(III) and potassium tris(oxalato) aluminate(III) trihydrate-reinvestigation. *Aust. J. Chem.* **1978**, *31*, 1455–1462.
34. Bulc, N.; Golic, L.; Siftar, J. Structure of ammonium tris(oxalato)gallate(III) trihydrate, (I) $(NH_4)_3[Ga(C_2O_4)_3].3H_2O$, and ammonium tris(oxalato)aluminate(III) trihydrate, (II) $(NH_4)_3[Al(C_2O_4)_3].3H_2O$. *Acta Cryst. C* **1984**, *40*, 1829–1831.
35. Chohan, S.; Pritchard, R.G. Tripotassium tris(oxalato-κ^2O,O')-aluminate bis(hydrogen peroxide) hydrate, the first example of a cyclic hydrogen-bonded H_2O_2 dimer. *Acta Cryst. C* **2003**, *59*, m187–m189.
36. Pellaux, R.; Decurtins, S.; Schmalle, H.W. Three anionic polymeric networks: Sodium(I)-ruthenium(III), sodium(I)-rhodium(III) and sodium(I)-aluminium(III) μ-oxalato complexes with tris(2,2'-bipyridine)ruthenium(II) cations. *Acta Cryst. C* **1999**, *55*, 1075–1079.
37. Martin, L.; Turner, S.S.; Day, P.; Guionneau, P.; Howard, J.A.; Hibbs, D.E.; Light, M.E.; Hursthouse, M.B.; Uruichi, M.; Yakushi, K. Crystal chemistry and physical properties of superconducting and semiconducting charge transfer salts of the type $(BEDT\text{-}TTF)_4[A^IM^{III}(C_2O_4)_3]\cdot PhCN$ (A^I = H_3O, NH_4, K; M^{III} = Cr, Fe, Co, Al; BEDT-TTF = Bis(ethylenedithio)tetrathiafulvalene). *Inorg. Chem.* **2001**, *40*, 1363–1371.
38. Bulc, N.; Golic, L.; Siftar, J. Structure of sodium trisoxalatoaluminate(III) pentahydrate and sodium trisoxalatochromate(III) pentahydrate, $Na_3[Al(C_2O_4)_3]\cdot 5H_2O$ and $Na_3[Cr(C_2O_4)_3]\cdot 5H_2O$. *Vestn. Slov. Kem. Drus.* (*Bull. Slov. Chem. Soc.*) **1982**, *29*, 211–215.
39. Golič, L.; Leban, I.; Bulc, N. The structure of sodium bis(tetraethylammonium) tris(oxalato)aluminate(III) monohydrate. *Acta Cryst. C* **1989**, *45*, 44–46.

40. Tapparo, A.; Heath, S.L.; Jordan, P.A.; Moore, G.R.; Powell, A.K. Crystal structure and solution-state study of $K[Al(mal)_2(H_2O)_2]\cdot 2H_2O$ (H_2mal = malonic acid). *J. Chem. Soc. Dalton Trans.* **1996**, 1601–1606.
41. Diaz-Acosta, I.; Baker, J.; Cordes, W.; Pulay, P. Calculated and experimental geometries and infrared spectra of metal tris-acetylacetonates: Vibrational spectroscopy as a probe of molecular structure for ionic complexes. Part I. *J. Phys. Chem. A* **2001**, *105*, 238–244.
42. Von Chrzanowski, L.S.; Lutz, M.; Spek, A.L. alpha-Tris(2,4-pentanedionato-κ^2O,O') aluminum(III) at 240, 210, 180, 150 and 110 K: A new delta phase at 110 K. *Acta Cryst. Sect. C* **2007**, *63*, m129.
43. Thurston, J.H.; Trahan, D.; Ould-Ely, T.; Whitmire, K.H. Toward a general strategy for the synthesis of heterobimetallic coordination complexes for use as precursors to metal oxide materials: synthesis, characterization, and thermal decomposition of $Bi_2(Hsal)_6\cdot M(Acac)_3$ (M = Al, Co, V, Fe, Cr). *Inorg. Chem.* **2004**, *43*, 3299–3305.
44. Alekseev, A.; Gromilov, S.; Baidina, I.; Stabnikov, P.; Prokuda, O. Synthesis of bimetallic complexes based on acetylacetonates of aluminum and ferrum. Crystalline structure $Al_{0.9}Fe_{0.1}(acac)_3$. *J. Struct. Chem.* **2006**, *47*, 318–325.
45. Le, Q.T.H.; Umetani, S.; Matsui, M. Ion-size recognition of Group 13 metals (Al^{3+}, In^{3+}) with modified-diketones. *J. Chem. Soc.*, *Dalton Trans.* **1997**, 3835–3840.
46. Zhang, C.; Yang, P.; Yang, Y.; Huang, X.; Yang, X.; Wu, B. High-yield synthesis of 1,3-dimesityl-propane-1,3-dione: Isolation of its aluminum complex as a stable intermediate. *Synth. Commun.* **2008**, *38*, 2349–2356.
47. Hori, A.; Shinohe, A.; Takatani, S.; Miyamoto, T.K. Synthesis and crystal structures of fluorinated β-diketonate metal (Al^{3+}, Co^{2+}, Ni^{2+} and Cu^{2+}) complexes. *Bull. Chem. Soc. Jpn.* **2009**, *82*, 96–98.
48. Neelgund, G.M.; Shivashankar, S.A.; Narasimhamurthy, T.; Ng, S.W. Tris(methyl 3-oxobutanoato-κ^2O,O')aluminium(III). *Acta Cryst. E* **2009**, *65*, m1681.
49. Dharmaprakash, M.S.; Thamotharan, S.; Neelgundc, G.M.; Shivashankarc, S.A. Tris(*tert*-butyl 3-oxobutanoato-κ^2O^1,O^3)-aluminium (III) at 153 K. *Acta Cryst. E* **2006**, *62*, m434–m436.
50. Vreshch, V.D.; Lysenko, A.B.; Chernega, A.N.; Howard, J.A.; Krautscheid, H.; Sieler, J.; Domasevitch, K.V. Extended coordination frameworks incorporating heterobimetallic squares. *Dalton Trans.* **2004**, 2899–2903.
51. Lutz, T.G.; Clevette, D.J.; Rettig, S.J.; Orvig, C. Metal chelation with natural products: Isomaltol complexes of aluminum, gallium, and indium. *Inorg. Chem.* **1989**, *28*, 715–719.
52. Yu, P.; Phillips, B.L.; Olmstead, M.M.; Casey, W.H. Rates of solvent exchange in aqueous aluminium(iii)-maltolate complexes. *J. Chem. Soc.*, *Dalton Trans.* **2002**, 2119–2125.
53. Odoko, M.; Yamamoto, K.; Hosen, M.; Okabe, N. *fac*-Tris(2-ethyl-4-oxo-4*H*-pyran-3-olato-κ^2O^3,O^4) iron (III) and its aluminium (III) analog. *Acta Cryst. C* **2003***, 59*, m121–m123.
54. Karpishin, T.B.; Stack, T.D.; Raymond, K.N. Octahedral *versus* trigonal prismatic geometry in a series of catechol macrobicyclic ligand-metal complexes. *J. Am. Chem. Soc.* **1993***, 115*, 182–192.
55. Di Marco, V.B.; Bombi, G.; Tapparo, A.; Powell, A.K.; Anson, C.E. Complexation of aluminium(III) with 3-hydroxy-2(1*H*)-pyridinone. Solution state study and crystal structure of tris(3-hdroxy-2(1*H*)-pyridinonato)aluminium(III). *J. Chem. Soc.*, *Dalton Trans.* **1999**, 2427–2432.

56. Nelson, W.O.; Rettig, S.J.; Orvig, C. Exoclathrate $Al(C_7H_8NO_2)_3.12H_2O$. A facial geometry imposed by extensive hydrogen bonding with the ice I structure. *J. Am. Chem. Soc.* **1987**, *109*, 4121–4123.
57. Nelson, W.O.; Karpishin, T.B.; Rettig, S.J.; Orvig, C. Aluminum and gallium compounds of 3-hydroxy-4-pyridinones: synthesis, characterization, and crystallography of biologically active complexes with unusual hydrogen bonding. *Inorg. Chem.* **1988**, *27*, 1045–1051.
58. Simpson, L.; Rettig, S.J.; Trotter, J.; Orvig, C. 1-*n*-Propyl-and 1-*n*-butyl-3-hydroxy-2-methyl-4-pyridinone complexes of group 13 (IIIA) metal ions. *Can. J. Chem.* **1991**, *69*, 893–900.
59. Zhang, Z.; Rettig, S.J.; Orvig, C. Lipophilic coordination compounds: aluminum, gallium, and indium complexes of 1-aryl-3-hydroxy-2-methyl-4-pyridinones. *Inorg. Chem.* **1991**, *30*, 509–515.
60. Muetterties, E.L.; Guggenberger, L.J. Stereochemically nonrigid six-coordinate molecules. Crystal structure of tris(tropolonato)aluminum(III). *J. Am. Chem. Soc.* **1972**, *94*, 8046–8055.
61. Nomiya, K.; Yoshizawa, A.; Tsukagoshi, K.; Kasuga, N.C.; Hirakawa, S.; Watanabe, J. Synthesis and structural characterization of silver(I), aluminium(III) and cobalt(II) complexes with 4-isopropyltropolone (hinokitiol) showing noteworthy biological activities. Action of silver(I)-oxygen bonding complexes on the antimicrobial activities. *J. Inorg. Biochem.* **2004***, 98*, 46–60.
62. Xu, J.; Parac, T.N.; Raymond, K.N. Meso myths: What drives assembly of helical *versus meso*-$[M_2L_3]$ clusters? *Angew. Chem. Int. Ed.* **1999**, *38*, 2878–2882.
63. Wunderlich, C.H.; Bergerhoff, G. Crystal structure of di-μ-oxo-bis(bis(1,2-dihydroxyanthrachinonato)aluminium-(aquabis(dimethylformamide)calcium)), $Al_2O_4(C_{14}H_6O_4)_4$ $Ca_2(HCON\ (CH_3)_2)_4(H_2O)_2$,(alizarine complex). *Z. Kristallogr.* **1993**, *207*, 185–188.
64. Bergerhoff, G.; Wunderlich, C.H. Crystal structure of di-μ-oxo-bis(bis(1,2,4-trihydroxyanthrachinonato)aluminium-(aquabis(dimethylformamide)calcium)), $Al_2O_4(C_{14}H_6O_5)_4$ $Ca_2(HCON(CH_3)_2)_4(H_2O)_2$, (purpurine complex). *Z. Kristallogr.* **2010**, *207*, 189–192.
65. Venema, F.R.; van Koningsveld, H.; Peters, J.A.; van Bekkum, H. Co-operative hydrogen bonding with short O O distances in a binuclear Al-glycolate complex. *J. Chem. Soc.*, *Chem. Commun.* **1990**, 699–700.
66. Van Koningsveld, H.; Venema, F.R. Structure of the hydrogen-bonded binuclear complex trisodium trihydrogen bis[tris(glycolato)aluminate(III)]. *Acta Cryst. C* **1991**, *47*, 289–292.
67. Bombi, G.G.; Corain, B.; Sheikh-Osman, A.A.; Valle, G.C. The speciation of aluminum in aqueous solutions of aluminum carboxylates. Part I. X-ray molecular structure of $Al[OC(O)CH(OH)CH_3]_3$. *Inorg. Chim. Acta* **1990**, *171*, 79–83.
68. Matzapetakis, M.; Raptopoulou, C.P.; Terzis, A.; Lakatos, A.; Kiss, T.; Salifoglou, A. Synthesis, structural characterization, and solution behavior of the first mononuclear, aqueous aluminum citrate complex. *Inorg. Chem.* **1999**, *38*, 618–619.
69. Matzapetakis, M.; Kourgiantakis, M.; Dakanali, M.; Raptopoulou, C.P.; Terzis, A.; Lakatos, A.; Kiss, T.; Banyai, I.; Iordanidis, L.; Mavromoustakos, T.; *et al*. Synthesis, pH-dependent structural characterization, and solution behavior of aqueous aluminum and gallium citrate complexes. *Inorg. Chem.* **2001**, *40*, 1734–1744.

70. Dakanali, M.; Raptopoulou, C.P.; Terzis, A.; Lakatos, A.; Banyai, I.; Kiss, T.; Salifoglou, A. A novel dinuclear species in the aqueous distribution of aluminum in the presence of citrate. *Inorg. Chem.* **2003**, *42*, 252–254.
71. Feng, T.L.; Gurian, P.L.; Healy, M.D.; Barron, A.R. Aluminum citrate: Isolation and structural characterization of a stable trinuclear complex. *Inorg. Chem.* **1990**, *29*, 408–411.
72. Keizer, T.S.; Scott, B.L.; Sauer, N.N.; McCleskey, T.M. Stable, soluble beryllium aluminum citrate complexes inspired by the emerald mineral structure. *Angew. Chem. Int. Ed.* **2005**, *44*, 2403–2406.
73. Happel, O.; Harms, K.; Seubert, A. Synthesis and structural characterization of two aluminium malate complexes. *Z. Anorg. Allg. Chem.* **2007**, *633*, 1952–1958.
74. Lakatos, A.; Bertani, R.; Kiss, T.; Venzo, A.; Casarin, M.; Benetollo, F.; Ganis, P.; Favretto, D. Al^{III} ion complexes of saccharic acid and mucic acid: A solution and solid-state study. *Chem. Eur. J.* **2004**, *10*, 1281–1290.
75. Klüfers, P.; Kramer, G.; Piotrowski, H.; Senker, J. Polyol-Metall-Komplexe, 43 [1]. Galactarato-Komplexe mit Aluminium und Kupfer (II). *Z. Naturforsch. B* **2002**, *57*, 1446–1453.
76. Lewiński, J.; Zachara, J.; Grabska, E. Synthesis and molecular structure of (^{t}BuOO)(^{t}BuO)Al (μ-O^{t}Bu)$_2$Al(mesal)$_2$. The first structurally characterized (alkylperoxo)aluminum compound. *J. Am. Chem. Soc.* **1996**, *118*, 6794–6795.
77. Lewinski, J.; Zachara, J.; Gos, P.; Grabska, E.; Kopec, T.; Madura, I.; Marciniak, W.; Prowotorow, I. Reactivity of various four-coordinate aluminum alkyls towards dioxygen: Evidence for spatial requirements in insertion of an oxygen molecule into the Al–C bond. *Chem. Eur. J.* **2000**, *6*, 3215–3227.
78. Kessler, V.G.; Gohil, S.; Parola, S. Interaction of some divalent metal acetylacetonates with Al, Ti, Nb and Ta isopropoxides. Factors influencing the formation and stability of heterometallic alkoxide complexes. *Dalton Trans.* **2003**, 544–550.
79. Garbauskas, M.F.; Wengrovius, J.H. Structure of the aluminium alkoxide complex [Al(O-iPr)(3,5-heptanedione)$_2$]$_2$. *Acta Cryst. C* **1987**, *43*, 2441–2442.
80. Cohen, S.M.; Raymond, K.N. Catecholate/salicylate heteropodands: Demonstration of a catecholate to salicylate coordination change. *Inorg. Chem.* **2000**, *39*, 3624–3631.
81. Cohen, S.M.; Meyer, M.; Raymond, K.N. Enterobactin protonation and iron Release: Hexadentate tris-salicylate ligands as models for triprotonated ferric enterobactin1. *J. Am. Chem. Soc.* **1998**, *120*, 6277–6286.
82. Polynova, T.N.; Bel'skaya, N.P.; de Garciya Banus, D.T.; Porai-Koshits, M.A.; Martynenko, L.I. Crystal structure of the dihydrated potassium salt of aluminum ethylenediaminetetraacetate. *J. Struct. Chem.* **1970**, *11*, 158–159.
83. Polynova, T.N.; Zasurskaya, L.A.; Ilyukhin, A.B. Redetermination of the crystal structure of K[AlEdta].2H$_2$O. *Crystallogr. Rep.* **1997**, *42*, 168.
84. Jung, W.S.; Chung, Y.K.; Shin, D.M.; Kim, S.D. Crystal and solution structure characteristics of ethylenediaminetetraacetatoaluminate(III) and gallate(III). *Bull. Chem. Soc. Jpn.* **2002**, *75*, 1263–1267.
85. Petrosyants, S.P.; Ilyukhin, A.B.; Malyarik, M.A. Hydrogen-bonded aggregates of scandium(III) complexes. *Russ. J. Inorg. Chem.* **1996**, *41*, 1595.

86. Schmitt, W.; Jordan, P.A.; Henderson, R.K.; Moore, G.R.; Anson, C.E.; Powell, A.K. Synthesis, structures and properties of hydrolytic Al(III) aggregates and Fe(III) analogues formed with iminodiacetate-based chelating ligands. *Coord. Chem. Rev.* **2002**, *228*, 115–126.
87. Kilyen, M.; Lakatos, A.; Latajka, R.; Labadi, I.; Salifoglou, A.; Raptopoulou, C.P.; Kozlowski H.; Kiss T. Al(III)-binding properties of iminodiacetic acid, nitrilotriacetic acid and their mixed carboxylic-phosphonic derivatives. *J. Chem. Soc.*, *Dalton Trans.* **2002**, 3578–3586.
88. Ilyukhin, A.B.; Petrosyants, S.P.; Millovanov, S.V.; Malyarik, M.A. Aluminum(III) and gallium(III) complexes with methyliminodiacetic acid: Crystal structures of $Cat[M(Mida)_2]$ (Cat^+ = Na, K, NH_4; M^{3+} = Al, Ga) and $M_4N[Ga(Mida)_2]H_2O$. *Crystallogr. Rep.* 1997, *42* 958–965.
89. Petrosyants, S.P.; Malyarik, M.A.; Ilyukhin, A.B. Complexation of aluminium and gallium with iminodiacetic acid in aqueous solutions: Crystal structure of diaqua di-μ-hydroxobis (iminodiacetato)di aluminium(III) and potassium bis(iminodiacetato)gallate(III). *Russ. J. Inorg. Chem.* **1995**, *40*, 765.
90. Jyo, A.; Kohno, T.; Terazono, Y.; Kawano, S. Crystal structure of the aluminum(III) complex of 1,4,7-Triazacyclononane-*N*,*N*',*N*''-triacetate. *Anal. Sci.* **1990**, *6*, 629–630.
91. Bossek, U.; Hanke, D.; Wieghardt, B.K. Pendent arm macrocyclic complexes: Crystal structures of Al(TCTA) and In (TS-TACN). *Polyhedron* **1993**, *12*, 1–5.
92. Soleimannejad, J.; Aghabozorg, H.; Mohammadzadeh, Y.; Hooshmand, S. 2-(2-Pyridyl) pyridinium bis(pyridine-2,6-dicarboxylato-κ^3O,N,O')aluminate(III) trihydrate. *Acta Cryst.* **2008**, *E64*, m870–m871.
93. Valle, G.C.; Bombi, G.G.; Corain, B.; Favarato, M.; Zatta, P. Crystal and molecular structures of diaqua(nitrilotriacetato)aluminium(III) and di-μ-hydroxo-bis(nitrilotriacetato)dialuminate(III) dianion. *J. Chem. Soc. Dalton Trans.* **1989**, 1513–1517.
94. Heath, S.L.; Jordan, P.A.; Johnson, I.D.; Moore, G.R.; Powell, A.K.; Helliwell, M. Comparative X-ray and ^{27}Al NMR spectroscopic studies of the speciation of aluminum in aqueous systems: Al(III) complexes of $N(CH_2CO_2H)_2(CH_2CH_2OH)$. *J. Inorg. Biochem.* **1995**, *59*, 785–794.
95. Joszai, R.; Kerekes, I.; Satoshi, I.; Sawada, K.; Zekany, L. Equilibrium and structure of the Al(III)-ethylenediamine-*N*,*N*'-bis(3-hydroxy-2-propionate) (EDBHP) complex. A multi-method study by potentiometry, NMR, ESI MS and X-ray diffraction. *Dalton Trans.* **2006**, 3221–3227.
96. Rajeswaran, M.; Blanton, T.N.; Klubek, K.P. Refinement of the crystal structure of the δ-modification of tris(8-hydroxy-quinoline)aluminum(III), δ-$Al(C_9H_6NO)_3$, the blue luminescent Alq_3. *Z. Kristallogr.* **2003**, *218*, 439–440.
97. Muccini, M.; Loi, M.A.; Kenevey, K.; Zamboni, R.; Masciocchi, N.; Sironi, A. Blue luminescence of facial tris(quinolin-8-olato)aluminum (III) in solution, crystals, and thin films. *Adv. Mater.* **2004**, *16*, 861–864.
98. Rajeswaran, M.; Blanton, T.N. Structure determination of a new polymorph (ε-Alq_3) of the electroluminescence OLED (organic light-emitting diode) material, tris(8-hydroxyquinoline) aluminum(Alq_3). *J. Chem. Cryst.* **2005**, *35*, 71–76.
99. Kim, T.S.; Kim, D.H.; Im, H.J.; Shimada, K.; Kawajiri, R.; Okubo, T.; Murata, H.; Mitani, T. Improved lifetime of an OLED using Aluminum(III) tris(8-hydroxyquinolate). *Sci. Tech. Adv. Mater.* **2004**, *5*, 331–337.

100. Fujii, I.; Hirayama, N.; Ohtani, J.; Kodama, K. Crystal structure of tris(8-quinolinolato) aluminum(III)-ethyl acetate (1/0.5). *Anal. Sci.* **1996**, *12*, 153–154.
101. Yuchi, A.; Hiramatsu, H.; Ohara, M.; Ohata, N. Performance of tris(2-methyl-8-quinolinolato) aluminum as fluorescent anionophore. *Anal. Sci.* **2003**, *19*, 1177–1181.
102. Iijima, T.; Yamamoto, T. Synthesis of reactive $[Al(Et)(q')_2]$(q' = 2-methyl-8-quinolinolato) serving as a precursor of light emitting aluminum complexes: Reactivity, optical properties, and fluxional behavior of the aluminum complexes. *J. Organometal. Chem.* **2006**, *691*, 5016–5023.
103. Amini, M.M.; Sharbatdaran, M.; Mirzaeeand, M.; Mirzaei, P. Synthesis, structure and luminescence study of a binuclear aluminium complex: A novel structure containing six coordinated aluminium atoms in two distinct coordination geometries. *Polyhedron* **2006**, *25*, 3231–3237.
104. Albrecht, M.; Blau, O.; Fröhlich, R. Supramolecular chemistry and self-assembly special feature: "Size-selectivity" in the template-directed assembly of dinuclear triple-stranded helicates. *Proc. Natl. Acad. Sci. USA* **2002**, *99*, 4867.
105. Dawson, A.; Wang, J.F.; Carducci, M.D.; Mash, E.A. Tris[2-(2-oxidophenyl)-5-phenyl-1,3,4-oxadiazole-κ^2O^2,N^3]aluminium 0.167-hydrate. *Acta Cryst.* **2004**, *E60*, m1644–m1646.
106. Steinhauser, S.; Heinz, U.; Bartholomä, M.; Weyhermüller, T.; Nick, H.; Hegetschweiler, K. Complex formation of ICL670 and related ligands with Fe^{III} and Fe^{II}. *Eur. J. Inorg. Chem.* **2004**, 4177–4192.
107. Jegier, J.A.; Munoz-Hernandez, M.; Atwood, D.A. Six-coordinate aluminium cations: Synthesis, characterization and catalysis. *J. Chem. Soc. Dalton Trans.* **1999**, 2583–2588.
108. Ikeda, C.; Ueda, S.; Nabeshima, T. Aluminium complexes of N_2O_2-type dipyrrins: the first hetero-multinuclear complexes of metallo-dipyrrins with high fluorescence quantum yields. *Chem. Commun.* **2009**, 2544–2546.
109. Cissell, J.A.; Vaid, T.P.; Rheingold, A.L. Aluminum tetraphenylporphyrin and aluminum phthalocyanine neutral radicals. *Inorg. Chem.* **2006**, *45*, 2367–2369.
110. Camacho-Camacho, C.; Merino, G.; Martínez-Martínez, F.J.; Nöth, H.; Contreras, R. Syntheses and characterization by NMR spectroscopy and X-ray diffraction of complexes derived from metals of groups 2 and 13 and the ligand bis (3,5-di-*tert*-butyl-1-hydroxy-2-phenyl) amine. *Eur. J. Inorg. Chem.* **1999**, 1021–1027.
111. Qiao, J.; Wang, L.D.; Xie, J.F.; Lei, G.T.; Wu, G.S.; Qiu, Y. Strongly luminescent binuclear aluminium chelate with polymer-like molecular packing and solution processibility. *Chem. Commun.* **2005**, 4560–4562.
112. Tong, Y.P.; Zheng, S.L.; Chen, X.M. Syntheses, structures, and luminescent properties of isomorphous hydroxo-bridged aluminum(III) and indium(III) compounds with 2-(2-hydroxyphenyl) benzimidazole. *Aust. J. Chem.* **2006**, *59*, 653–656.
113. Hoveyda, H.R.; Rettig, S.J.; Orvig, C. Coordination chemistry of 2-(2'-hydroxyphenyl)-2-benzoxazole with gallium(III) and aluminum(III): Two uncommon Group 13 metal environments stabilized by a biologically relevant binding group. *Inorg. Chem.* **1993**, *32*, 4909–4913.
114. Langemann, K.; Heineke, D.; Rupprecht, S.; Raymond, K.N. Nordesferriferrithiocin. Comparative coordination chemistry of a prospective therapeutic iron chelating agent. *Inorg. Chem.* **1996**, *35*, 5663–5673.

115. Van Der Helm, D.; Baker, J.R.; Loghry, R.A.; Ekstrand, J.D. Structures of alumichrome A and ferrichrome A at low temperature. *Acta Cryst.* **1981**, *B37*, 323–330.
116. Liu, S.; Rettig, S.J.; Orvig, C. Polydentate ligand chemistry of Group 13 metals: Effects of the size and donor selectivity of metal ions on the structures and properties of aluminum, gallium, and indium complexes with potentially heptadentate (N_4O_3) amine phenol ligands. *Inorg. Chem.* **1992**, *31*, 5400–5407.
117. Bekaert, A.; Lemoine, P.; Brion, J.D.; Viossat, B. Tris[(*R*)-lactamide-κ^2*O*,*O*']zinc(II) tetrabromozincate. *Z. Kristallogr.* **2006**, *221*, 45.
118. Babian-Kibala, E.; Chen, H.; Cotton, F.A.; Daniels, L.M.; Falvello, L.R.; Schmid, G.; Yao, Z. Synthesis and problematic crystal structures of $[Al(CH_3CN)_6][MCl_6]_3(CH_3CN)_3$ (M = Ta, Nb or Sb). *Inorg. Chim. Acta* **1996**, *250*, 359–364.
119. Pfeiffer, M.; Murso, A.; Mahalakshmi, L.; Moigno, D.; Kiefer, W.; Stalke, D. Experimental and computational study on a variety of structural motifs and coordination modes in aluminium complexes of di(2-pyridyl)amides and -phosphanides. *Eur. J. Inorg. Chem.* **2002**, *2002*, 3222–3234.
120. Leman, J.T.; Braddock-Wilking, J.; Coolong, A.J.; Barron, A.R. 1,3-Diaryltriazenido compounds of aluminum. *Inorg. Chem.* **1993**, *32*, 4324–4336.
121. Braddock-Wilking, J.; Leman, J.T.; Farrar, C.T.; Cosgrove-Larsen, S.A.; Singel, D.J.; Barron, A.R. Radical anion complexes of tris(1,3-diphenyltriazenido)aluminum. *J. Am. Chem. Soc.* **1995**, *117*, 1736–1745.
122. Chen, P.; Li, J.; Xu. J.; Duang, F.; Deng, F.; Xu. R. Synthesis, structure and NMR characterization of a new monomeric aluminophosphate $[dl\text{-}Co(en)_3]_2[Al(HPO_4)_2(H_{1.5}PO_4)_2(H_2PO_4)_2](H_3PO_4)_4$ containing four different types of monophosphates. *Solid Sate Sci.* **2009**, *11*, 622–627.
123. Azais, T.; Bonhomme, C.; Bonhomme-Coury, L.; Vaissermann, J.; Millot, Y.; Man, P.P.; Bertani, P.; Hirschinger, J.; Livage, J. Cubane shaped clusters, precursors for aluminophosphate frameworks: A solid state multinuclear NMR study, in time and frequency domains. *J. Chem. Soc. Dalton Trans.* **2002**, 609–618.
124. Azaïs, T.; Bonhomme-Coury, L.; Vaissermann, J.; Bertani, P.; Hirschinger, J.; Maquet, J.; Bonhomme, C. Synthesis and characterization of a novel cyclic aluminophosphinate: Structure and solid-state NMR study. *Inorg. Chem.* **2002**, *41*, 981–988.
125. Azaïs, T.; Bonhomme-Coury, L.; Vaissermann, J.; Maquet, J.; Bonhomme, C. The first aluminophosphonate cluster analogue of the 4=1 SBU of zeolites: Structure and multinuclear solid-state NMR study, including ^{1}H NMR. *Eur. J. Inorg. Chem.* **2002**, 2838–2843.
126. Azais, T.; Bonhomme, C.; Bonhomme-Coury, L.; Kickelbick, G. Aluminophosphonate clusters: A new architecture. *Dalton Trans.* **2003**, 3158–3159.
127. Grottel, M.; Kozak, A.; Maluszyriska, H.; Pajak, Z. An X-ray and nuclear magnetic resonance study of structure and ion motions in $(C(NH_2)_3)_3AlF_6$. *J. Phys.* **1992**, *4*, 1837.
128. Adil, K.; Goreshnik, E.; Courant, S.; Dujardin, G.; Leblanc, M.; Maisonneuve, V. Synthesis and structures of new hybrid fluorides templated by tetraprotonated pentaerythrityl tetramine. *Solid State Sci.* **2004**, 1229–1235.
129. Adil, K.; Leblanc, M.; Maisonneuve, V. Structural chemistry of organically-templated metal fluorides. *J. Fluorine Chem.* **2006**, *127*, 1349–1354.

130. Bourosh, P.N.; Koropchanu, E.B.; Simonov, Y.; Gdaniec, M.; Bologa, O.A.; Gerbeleu, N.V. Cobalt(III) α-dimethylglyoximates $[Co(DH)_2(Py)_2]_2SiF_6 \cdot 10H_2O$ and $[Co(DH)_2(Thio)_2]_2SiF_6 \cdot 2H_2O \cdot C_2H_5OH$: Synthesis and structure. *Russ. J. Inorg. Chem.* **2002**, *7*, 1604.
131. Touret, J.; Bourdon, X.; Leblanc, M.; Retoux, R.; Renaudin, J.; Maisonneuve, V. Crystal structure of new hydroxide fluorides with isolated F-anions: $[H_3N(CH_2)_6NH_3]_2M(F,OH)_6(F,OH) \cdot H_2O$ (M = Al, In). *J. Fluorine Chem.* **2001**, *110*, 133–138.
132. Adil, K.; Marrot, J.; Leblanc, M.; Maisonneuve, V. Diethylenetriaminium hexafluoroaluminate dehydrate. *Acta Cryst.* **2005**, *E61*, m1178–m1180.
133. Fourquet, J.L.; Plet, F.; Paper, R.D. The structure of dimercury(I) alluminium(III) fluoride dehydrate. *Rev. Chim. Miner.* **1986**, *23*, 183.
134. Goreshnik, E.; Leblanc, M.; Maisonneuve, V. 1,4,8,11-Tetraazacyclodecane-1,4,8,11-tetraium bis(aquapentafluoroaluminate) dehydrate. *Acta Cryst.* **2003**, *E59*, m1059–m1061.
135. Cadiau, A.; Hemon-Ribaud, A.; Leblanc, M.; Maisonneuve, V. 2,4,6-Triamino-1,3,5-triazine-1,3-diium aquapentafluoridoaluminate. *Acta Cryst.* **2008**, *E64*, m523–m524.
136. Adil, K.; Leblanc, M.; Maisonneuve, V. Tris(2-ammonioethyl)aminium decafluorominium monohydrate, $(H_4tren)[Al_2F_{10}] \cdot H_2O$. *Acta Cryst.* **2004**, *E60*, m1379–m1381.
137. Tang, L.Q.; Dadachov, M.S.; Zou, X.D. SU-12: A silicon-substituted ASU-16 with circular 24-rings and templated by a monoamine. *Z. Kristallogr.* **2001**, *216*, 385–386.
138. Goreshnik, E.; Leblanc, M.; Maisonneuve, V. From isolated polyanions to 1-D structure: Synthesis and crystal structure of hybrid fluorides $\{[(C_2H_4NH_3)_3NH]^{4+}\}_2 \cdot (H_3O)^+ \cdot [Al_7F_{30}]^{9-}$ and $\{[(C_2H_4NH_3)_3NH]_4^+\}_2 \cdot [Al_7F_{29}]^{8-} \cdot (H_2O)_2$. *Z. Anorg. Allg. Chem.* **2002**, *628*, 162–166.
139. Dimitrov, A.; Heidemann, D.; Kemnitz, E. F/Cl-Exchange on $AlCl_3$-pyridine adducts: Synthesis and characterization of *trans*-difluoro-tetrakis-pyridine-aluminum-chloride, $[AlF_2(Py)_4]^+Cl^-$. *Inorg. Chem.* **2006**, *45*, 10807–10814.
140. Krossing, I.; Raabe, I. Noncoordinating anions—Fact or fiction? A survey of likely candidates. *Angew. Chem. Int. Ed.* **2004**, *43*, 2066–2090.
141. Gonsior, M.; Krossing, I.; Müller, L.; Raabe, I.; Jansen, M.; van Wüllen, L. PX_4^+, $P_2X_5^+$, and $P_5X_2^+$ (X = Br, I) salts of the superweak $Al(OR)_4^-$ anion [R = $C(CF_3)_3$]. *Chem. Eur. J.* **2002**, *8*, 4475–4492.
142. Krossing, I. The facile preparation of weakly coordinating anions: Structure and characterisation of silverpolyfluoroalkoxyaluminates $AgAl(OR_F)_4$, calculation of the alkoxide ion affinity. *Chem. Eur. J.* **2001**, *7*, 490–502.
143. Santiso-Quiñones, G.; Brückner, R.; Knapp, C.; Dionn, I.; Passmore, J.; Krossing, I. Cyclododecasulfur as a ligand: From gas-phase experiments to the crystal structures of $[Cu(S_{12})(S_8)]^+$ and $[Cu(S_{12})(CH_2Cl_2)]^+$. *Angew. Chem. Int. Ed.* **2009**, *48*, 1133–1137.
144. Santiso-Quiñones, G.; Higelin, A.; Schaefer, J.; Brückner, R.; Knapp, C.; Krossing, I. $Cu[Al(OR^F)_4]$ starting materials and their application in the preparation of $[Cu(S_n)]^+$ (n = 12, 8) complexes. *Chem. Eur. J.* **2009**, *15*, 6663–6677.
145. Lewinski, J.; Zachara, J.; Kopec, T.; Madura, I.; Prowotorow, I. On the mechanism of four-coordinate aluminum alkyls interaction with dioxygen: Evidence for spatial demands in the autoxidation reaction. *Inorg. Chem. Commun.* **1999**, *2*, 131–134.

146. Kendall, R.A.; Dunning, T.H., Jr.; Harrison, R.J. Electron affinities of the first-row atoms revisited. Systematic basis sets and wave functions. *J. Chem. Phys.* **1992**, *96*, 6796–6806.
147. Woon, D.E.; Dunning, T.H., Jr. Gaussian basis sets for use in correlated molecular calculations. III. The second row atoms, Al-Ar. *J. Chem. Phys.* **1993**, *98*, 1358–1371.
148. Haraguchi, H.; Fujiwara, S. Aluminum complexes in solution as studied by aluminum-27 nuclear magnetic resonance. *J. Phys. Chem.* **1969,** *78*, 3467–3473.
149. Kon'shin, V.V.; Chernyshov, B.N.; Ippolitov, E.G. Composition and structure of aluminum fluorocomplexes in aqueous solutions of hydrogen peroxide and inorganic acids. *Russ. Chem. Bull.* **1987**, *36*, 1577–1581.
150. Müller, D.; Bentrup, U. ^{27}Al-NMR-Untersuchungen an Alkalifluoroaluminaten. *Z. Anorg. Allg. Chem.* **1989**, *575*, 17–25.
151. Chen, J.L.; Noodleman, L.; Case D.A.; Bashford, D. Incorporating solvation effects into density functional electronic structure calculations. *J. Phys. Chem.* **1994**, *98*, 11059–11068.
152. Tomasi, J.; Mennucci, B.; Cammi, R. Quantum mechanical continuum solvation models. *Chem. Rev.* **2005**, *105*, 2999–3093.
153. Frisch, M.J.; Trucks, G.W.; Schlegel, H.B.; Scuseria, G.E.; Robb, M.A.; Cheeseman, J.R.; Montgomery, J.A., Jr.; Vreven, T.; Kudin, K.N.; Burant, J.C.; *et al*. Gaussian 03 Revision B.05; Gaussian Inc.: Wallingford, CT, USA, 2004.
154. Vosko, S.H.; Wilk, L.; Nusair, M. Accurate spin-dependent electron liquid correlation energies for local spin density calculations: a critical analysis. *Can. J. Phys.* **1980**, *58*, 1200–1211.
155. Stephens, P.J.; Devlin, F.J.; Chabalowski, C.F.; Frisch, M.J. *Ab initio* calculation of vibrational absorption and circular dichroism spectra using density functional force fields *J. Phys. Chem.* **1994**, *98*, 11623–11627.
156. Lee, C.; Yang, W.; Parr, R.G. Development of the Colle-Salvetti correlation-energy formula into a functional of the electron density. *Phys. Rev.* **1988**, *B37*, 785–789.
157. Becke, A.D. Density functional thermochemistry. III. The role of exact exchange. *J. Chem. Phys.* **1993**, *98*, 5648–5652.
158. Møller, C.; Plesset, M.S. Note on an approximation treatment for many-electron systems. *Phys. Rev.* **1934**, *46*, 618–622.
159. Francl, M.M.; Pietro, W.J.; Hehre, W.J.; Binkley, J.S.; Gordon, M.S.; DeFrees, D.J.; Pople, J.A. Self-consistent molecular orbital methods. 23. A polarization basis set for second row elements. *J. Chem. Phys.* **1982**, *77*, 3654–3665.
160. McLean, A.D.; Chandler, G.S. Contracted Gaussian basis sets for molecular calculations. I. Second row atoms, Z = 11–18. *J. Chem. Phys.* **1980**, *72*, 5639–5648.
161. Robinson, M.; Haynes, P.D. Dynamical effects in *ab initio* NMR calculations: Classical force fields fitted to quantum forces. *J. Chem. Phys.* **2010**, *133*, 084109.